Heliyon 10 (2024) e33687

Contents lists available at ScienceDirect

Heliyon

journal homepage: www.cell.com/heliyon

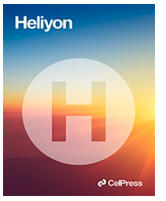

Research article

Identification of gemcitabine resistance-related AHNAK2 gene associated with prognosis and immune infiltration in pancreatic cancer

Guangsheng Ou [a,1], Zhenfeng Tian [b,c,1], Mingxin Su [b,c], Miao Yu [b,c], Jin Gong [d,**], Yinting Chen [b,c,*]

[a] Department of Gastrointestinal Surgery, the Third Affiliated Hospital of Sun Yat-Sen University, Guangzhou, 510600, PR China
[b] Guangdong Provincial Key Laboratory of Malignant Tumor Epigenetics and Gene Regulation, Sun Yat-Sen Memorial Hospital, Sun Yat-Sen University, Guangzhou, 510120, PR China
[c] Department of Gastroenterology, Sun Yat-Sen Memorial Hospital, Sun Yat-Sen University, Guangzhou, 510120, PR China
[d] Department of General Surgery, the First Affiliated Hospital of Jinan University, Guangzhou, 510632, PR China

ARTICLE INFO

Keywords:
Pancreatic cancer
AHNAK2
Gemcitabine
Immune infiltration
Resistance to chemotherapy

ABSTRACT

Purpose: Gemcitabine is a basic chemotherapy drug for pancreatic cancer (PC), but resistance is common and causes tumor recurrence and metastasis. Therefore, it is significant to explore gemcitabine resistance-related molecules for individualized treatment and prognosis assessment of PC.

Methods: In this study, transcriptome sequencing and TCGA database analysis were performed, and a differentiated gene AHNAK2 was screened. MEXPRESS database, tissue microarray analysis, and CIBERSORT and TIMER databases were used to correlate AHNAK2 expression with clinicopathological features and prognosis and immune infiltration of PC. Enrichment analysis was used to investigate the significant biological processes associated with AHNAK2.

Results: AHNAK2 was highly expressed in gemcitabine-resistant cells. High expression of AHNAK2 increased the risk of poor overall survival (OS) and progression-free survival (PFS) in PC. Clinicopathologic analysis revealed that AHNAK2 correlated with KRAS, TP53 mutations, histologic type, short OS, N stage, and elevated CA199 levels in PC. Knockdown of AHNAK2 inhibited the ability of cell proliferation and colony formation and enhanced the toxic effect of gemcitabine in PC. Meanwhile, the knockdown of AHNAK2 expression enhanced cell-ECM adhesion, inhibited cell-cell adhesion, and downregulated the KRAS/p53 signaling pathway in PC. Furthermore, AHNAK2 was correlated with immune infiltration, especially B cells and macrophages.

Conclusions: Our study unveils for the first time the pivotal role of AHNAK2 in PC, particularly its association with gemcitabine resistance, clinical prognosis, and immune infiltration. AHNAK2 not only drives the proliferation and drug resistance of PC cells by potentially activating the KRAS/p53 pathway but also significantly impacts cell-cell and cell- ECM adhesion. Additionally, AHNAK2 plays a crucial role in modulating the tumor immune microenvironment. These insights

* Corresponding author. Guangdong Provincial Key Laboratory of Malignant Tumor Epigenetics and Gene Regulation, Sun Yat-Sen Memorial Hospital, Sun Yat-Sen University, Guangzhou, 510120, PR China.
** Corresponding author.
E-mail addresses: gongjin153@163.com (J. Gong), chenyt58@mail.sysu.edu.cn (Y. Chen).
[1] These authors contributed equally to this work.

https://doi.org/10.1016/j.heliyon.2024.e33687
Received 18 March 2024; Received in revised form 25 June 2024; Accepted 25 June 2024
Available online 27 June 2024

underscore AHNAK2's unique potential as a novel therapeutic target for overcoming gemcitabine resistance, offering new perspectives for PC treatment strategies.

1. Introduction

Pancreatic cancer (PC) is a formidable disease with a dismal prognosis, displaying a 5-year survival rate of approximately 12 % [1]. In 2020, there were 496,000 new cases and 466,000 global deaths attributed to PC [2]. Surgery does provide the hope of more prolonged survival for patients with PC. However, at initial diagnosis, most patients have local progression or distant metastasis, and surgery is only suitable for 15%–20 % of cases [3]. Hence, there is an immediate need to explore alternative approaches for managing PC, which may involve non-surgical interventions such as chemotherapy or a combination of targeted medications and immunotherapy. Pancreatic ductal adenocarcinoma (PDAC) accounts for approximately 90 % of all PC cases. KRAS mutation occurs in more than 90 % of PDAC, which seems to be a good therapeutic target, but the therapeutic effect of targeting KRAS mutation and its key pathway is not ideal [4]. Immunotherapy has shown success in treating different forms of cancer, but when it comes to PC, most immunotherapy approaches have proven ineffective. This includes immune checkpoint inhibitors, CAR-T therapy, immunomodulators, and vaccines [5]. Therefore, chemotherapy is still the most important conventional treatment strategy for PC. Chemotherapy regimens based on the FOLFIRINOX regimen (oxaliplatin, leucovorin, irinotecan, and 5-fluorouracil) and gemcitabine are indicated for unresectable PC [6]. The high rate of chemotherapy resistance in PC is a significant challenge that limits the effectiveness of treatment and negatively impacts patient prognosis. To improve patient outcomes, it is crucial to understand the underlying mechanisms driving chemoresistance in PC thoroughly. By gaining insight into these mechanisms, developing more effective and targeted treatment regimens that can overcome chemoresistance and improve patient outcomes will be possible.

Gemcitabine is a deoxycytidine nucleoside analog, widely used as a first-line chemotherapeutic medication for PC. This medication acts by being phosphorylated, inhibiting both cell proliferation and cell cycle progression through the interference of DNA synthesis [7]. Gemcitabine resistance is common in PC, which has become an important entry point and hot spot in the study of chemotherapy resistance. Gemcitabine, an essential chemotherapeutic agent, is taken up by cells through the activity of nucleoside transporters (NTs). Two prominent types of NTs are involved in the cellular uptake of gemcitabine: the sodium-independent equilibrative nucleoside transporter (hENT) and the sodium-dependent concentrative nucleoside transporter (hCNT) [8]. Postoperative patients with high hENT expression had better prognoses after receiving gemcitabine-based chemotherapy [9]. Furthermore, a reduction in hCNT1 expression exhibited conformity with the advancement of tumors and resistance towards gemcitabine [10]. Regrettably, specific clinical trials focusing on transporters have encountered setbacks primarily due to the elevated toxicity and excessive drug concentrations in the bloodstream [11]. On entry into PC cells, gemcitabine is phosphorylated by deoxycytidine kinase (dCK) and then converted into the active variants of gemcitabine diphosphate (dFdCDP) and triphosphate (dFdCTP). dCK was post-transcriptionally regulated by RNA binding protein Hu antigen R (HuR). Cancer cells with high HuR expression are more sensitive to gemcitabine treatment [12]. Furthermore, inhibition of dFdCTP by ribonucleotide reductase (RR) is an important mechanism regulating the efficacy of gemcitabine [13]. Therefore, reagents targeting RR are potential options for PDAC with gemcitabine resistance accompanied by RR high expression. However, the molecular diagnostic markers and effective therapeutic targets closely related to gemcitabine resistance remain to be explored.

In addition to PC cells' intrinsic factors, tumor stromal components also play a significant role in chemosensitivity. The stromal component comprises 90 % of the overall PC tumor mass. On one hand, the dense fibrous stroma acts as a physical obstacle that hinders the entry of chemotherapy drugs into cancer cells. On the other hand, PC stromal components are complex, and multiple factors are known to be associated with the efficacy of PC chemotherapy and targeted therapy, such as signal redundancy, the role of stem cells, interstitial connective tissue hyperplasia and tumor microenvironment (TME) [14]. The TME is a complex and dynamic environment consisting of both cellular and non-cellular elements. These include fibroblasts, endothelial cells, immune cells, extracellular components such as growth factors, cytokines, and hormones, and an extracellular matrix. TME plays a crucial role in tumor initiation, progression, and metastasis, and it is a significant limiting factor in the efficacy of chemotherapy [15]. Stimulating and mobilizing the human immune system to enhance the anti-tumor ability of TME has emerged as a promising research direction for PC immunotherapy. PC Patients with a smaller volume of stromal cells and higher levels of peritumoral T lymphocytes, monocytes/macrophages, CTLA4, and PDL-1 experienced poorer overall survival (OS) [16–19]. Tumor-associated macrophages (TAMs) play a crucial role in regulating the response to TME treatment. TAMs have the capability to release various pyrimidines, including deoxycytidine, which compete with gemcitabine during drug uptake and metabolism, ultimately resulting in the enhancement of gemcitabine resistance [20]. Furthermore, TAMs induce peritoneal metastasis of PC cells and lead to gemcitabine resistance through the induction of epithelial-mesenchymal junctions (EMT) [21]. Interactions between cancer cells and their microenvironment lead to immune infiltration and immunosuppression of the pancreas, ultimately increasing tumor aggressiveness and compromising the effectiveness of drug therapy. The mechanism of immune infiltration and drug resistance in PC is urgently in need of investigation.

Focusing on the characteristics of pancreatic cancer resistant to gemcitabine, our study screened for differentially expressed genes associated with gemcitabine resistance by transcriptome sequencing and bioinformatics analysis and finally found that AHNAK2 was highly expressed in gemcitabine-resistant pancreatic cancer cell lines. AHNAK2 was first identified in 2004 as a 616 kDa protein composed of many highly conserved repeats [22]. Early studies have shown that AHNAK2 has the potential to be a future tumor biomarker and therapeutic target. However, due to the large molecular weight of AHNAK2, there are few studies on the function and relationship between AHNAK2 and cancer, and the role of AHNAK2 in malignant tumors is not yet fully understood. No studies have

explored its potential involvement in gemcitabine chemoresistance, immune infiltration, or treatment resistance in PC. In this study, we aim to examine the correlation between AHNAK2 and the clinicopathologic characteristics and prognosis of PC. Additionally, we will investigate the association between AHNAK2, immune checkpoint genes, immune regulatory genes, and immune infiltration in PC. This study provides important clinical data and experimental results for AHNAK2 as a therapeutic target for targeting the tumor immune microenvironment, enhancing chemotherapy sensitivity, and reversing drug resistance in PC.

2. Materials and methods

2.1. Cell lines and culture

We generated and cultured gemcitabine-resistant human pancreatic cancer MIA PaCa-2^{R} cells using the methodology detailed in our earlier research [23]. The cultivation procedure for human pancreatic cancer MIA PaCa-2 and MIA PaCa-2^{R} cells was also conducted in alignment with established literature guideline [23]. Firstly, we conducted IC50 testing of gemcitabine against the parental cell line MIA PaCa-2 and subsequently employed a method involving gradual increments in gemcitabine concentration to cultivate drug-resistant cell lines. Briefly, tumor cells in the logarithmic growth phase were exposed to an initial concentration of gemcitabine, one-tenth of the IC50 of the parental cell line. After a 24-h treatment period, the culture medium was discarded, and the cells were washed with PBS before being transferred to a gemcitabine-free medium for recovery and subsequent passaging. This process was repeated five times using the same concentration of gemcitabine until the cells displayed stable growth at this concentration. Subsequently, the gemcitabine concentration was incrementally increased until the cells could thrive in high-concentration gemcitabine environments. This process spanned over 6–8 months. Finally, by assessing the IC50 values of the cell lines and the parental cell line, successful construction of gemcitabine-resistant pancreatic cancer cell lines was confirmed if the ratio of the detected IC50 to that of the parental cell line exceeded 5.

2.2. Transcriptome sequencing

Transcriptome sequencing was carried out on MIA PaCa-2^{R} and MIA PaCa-2 cells, and differential analysis was executed employing the R packages limma (voom, lmFit, and eBayes functions), pheatmap and ggplot2. The data transformation was performed using the voom function, followed by linear modeling with the lmFit function and empirical Bayes analysis using the eBays function. Differentially expressed genes (DEGs) were pinpointed using criteria of $|\log FC| > 2$ and an adjusted P value < 0.01. Visualization of the expression patterns of all genes in the integrated matrix was carried out using the pheatmap R package. The DEGs were graphically represented via the ggplot2 R package to generate a volcano plot. These analytical methods illuminated noteworthy variations in gene expression between MIA PaCa-2^{R} and MIA PaCa-2 cells. All sequencing data are available through the NCBI Sequence Read Archive under the accession number PRJNA1088773 (https://dataview.ncbi.nlm.nih.gov/object/PRJNA1088773?reviewer=jckdiqn90cgh6af7dqd5jb4879).

2.3. GEO analysis

We obtained the GSE106336 microarray dataset from the GEO database, which consisted of six samples categorized into two distinct groups: the control group treated with PBS and the gemcitabine-treated group (GEM). Subsequently, we imported the dataset into R Studio software and removed genes with more than 50 % missing values to avoid bias. Gene expression values with repeated row names were processed using the median, followed by gene ID conversion. We performed differential analysis using limma on the GSE106336 chip. Differentially expressed genes were screened based on the criteria of HR > 1 and FDR <0.05.

2.4. TCGA database analysis

We acquired RNA-seq data along with corresponding clinical details for 178 PDAC samples from the TCGA database using UCSC Xena. Subsequently, survival analyses encompassing overall survival (OS) and progression-free survival (PFS) were conducted on these samples. A gene set meeting the criteria of HR > 1 and FDR <0.05 was subsequently identified. Utilizing this gene set, Venn diagrams were constructed, revealing genes that exhibited an elevated risk for an unfavorable prognosis in PC.

2.5. Cellular immunofluorescence

Before experimentation, a 12-well plate was prearranged with slides, each well accommodating 5×10^4 cells. Following 48 h of adhesion-driven growth, cells underwent a gentle rinse with PBS. Subsequently, they were fixed with 4 % paraformaldehyde, permeabilized using 0.5 % Triton X-100, and subjected to blockage with 5 % BSA. The cells were then subjected to incubation with anti-AHNKA2 antibody (Proteintech, diluted 1:500) overnight at 4 °C. After this step, secondary antibodies (Cell Signaling Technology, diluted 1:2000) were incubated at 37 °C in a dark environment for 1 h. For nuclear counterstaining, DAPI was employed, followed by sealing the slides using a mounting solution containing an anti-fluorescence quencher. Ultimately, observation and image capture were executed utilizing a fluorescence microscope.

2.6. Quantitative real-time reverse transcription PCR (qRT-PCR)

qRT-PCR was performed as we reported previously [23]. The GAPDH gene was used as a reference gene to normalize the specific gene mRNA expression. Primers used included: AHNAK2 forward (5′-3′): GTGCAGAAACGGAAGATGACC; AHNAK2 reverse (5′-3′): GCCTCAGTCGTGTATTCGTAGA; KRAS forward (5′-3′): ACAGAGAGTGGAGGATGCTTT; KRAS reverse (5′-3′): TTTCACA-CAGCCAGGAGTCTT; p53 forward (5′-3′): CAGCACATGACGGAGGTTGT; p53 reverse (5′-3′): TCATCCAAATACTCCACACGC.

2.7. siRNA-mediated AHNAK2 knocking down

AHNAK2 siRNA transfection was performed by using Lipofectamine 3000 (Invitrogen). The cells were then collected 72 h after siRNA transfection, and transfection efficacy was confirmed using qRT-PCR and cellular immunofluorescence. The sequences of AHNAK siRNA are as follows: siAHNAK2#1 (5′-3′): GUGUCCAGAGGCCAAUAUU; siAHNKA2#2 (5′-3′): CGCACAGAGGAAGGAUUAA.

2.8. AHNAK2 expression in human tumor samples

Leveraging the transcriptome sequencing findings of MIA PaCa-2^{R} and MIA PaCa-2 cells, along with the previously mentioned TCGA and GEO gene sets, we identified four differentially expressed genes, among which was AHNAK2. To obtain AHNAK2's gene expression data, we accessed the unified and standardized pan-cancer datasets available through the UCSC database. This included extracting AHNAK2 expression data from each sample and screening samples based on their respective source tissues. Samples with fewer than three instances for a specific cancer type were eliminated from the analysis. For each cancer type, we calculated expression differences between normal and tumor samples using R software (version 3.6.4). Subsequently, we utilized a chi-square test to evaluate differences in gene mutation frequency between the AHNAK2 low-expression and high-expression groups, and we visually presented the results as a gene mutation landscape map. Concerning PC cases within the TCGA database, we divided the samples into two groups: AHNAK2 low-expression and AHNAK2 high-expression groups, based on AHNAK2 gene expression levels.

2.9. MEXPRESS database analysis of AHNAK2 in pancreatic cancer

We performed a thorough analysis to investigate the correlation between AHNAK2 gene expression levels and the clinicopathological features of PC patients, utilizing the MEXPRESS database. Our study focused on PC patients from the TCGA database using the MEXEPRESS. To ensure reliable results, we excluded samples with a follow-up period of less than 30 days. This is crucial as it can compromise the accuracy of the overall survival (OS), disease-specific survival (DSS), disease-free interval (DFI), and progression-free interval (PFI) metrics. To evaluate the correlation between AHNAK2 gene expression levels and the survival metrics mentioned above, we utilized the log-rank method. This statistical approach allowed for analysis of the correlation between AHNAK2 gene expression and OS, DSS, DFI, and PFI. The results were presented visually using Kaplan-Meier (KM) curves.

2.10. Pancreatic cancer tissue microarray

Pancreatic cancer tissue chips with complete clinicopathological feature information were procured from Shanghai Xinchao Biotechnology Co., LTD. The microarray dataset encompassed 90 samples of PC tissues along with 80 corresponding adjacent normal tissues. The medical ethical approval number was SHYJS-CP-1901008.

2.11. Immunohistochemistry

After the tissue chips were dewaxed and hydrated, the sections were microwaved for 20 min in citrate or EDTA buffer to retrieve the antigen. Continuing the process, the slides were subjected to a 10-min pre-treatment with 3 % H_2O_2 at room temperature, followed by a 1-h incubation with 5 % goat serum for blocking under the same conditions. Perform another wash with PBST, then proceed to an overnight incubation at 4 °C using the anti-AHNAK2 antibody (Proteintech, Cat No.17682-1-AP). On the following day, after another round of PBST cleaning, introduce a secondary antibody conjugated with the chemiluminescent reporter enzyme horseradish peroxidase (HRP) and proceed with the incubation. After washing again, DAB was used to develop color, and hematoxylin was used to dye the slides. Finally, images were taken with a microscope. IHC results were scored according to the staining index. The staining index is defined as the multiplication of staining intensity and staining rate. The intensity is assessed using the following scoring criteria: negative (0 points), weak (1 point), moderate (2 points), and strong (3 points). Scale scores are 0 (no staining), 1 (1 %–25 %), 2 (26 %–50 %), 3 (51 %–75 %), and 4 (>75 %).

2.12. Cell proliferation

Cell proliferation was assessed using the Cell Counting Kit-8 (CCK-8) assay. Approximately 2000 cells were plated per well in a 96-well plate. At designated time points (0, 1, 2, 3, and 4 days post-inoculation), 10 μl of CCK-8 solution was added to each well. Following a 3-h incubation at 37 °C, the optical density of 450 nm was measured using a microplate reader.

2.13. Plate colony formation assay

Cell colony formation ability was evaluated using a plate colony formation assay. A total of 500 cells were seeded into each well of a 6-well plate and incubated for approximately 2 weeks until visible colonies formed. The plates were then gently washed and stained with crystal violet. The number of colonies was determined by counting the proliferating single cells.

2.14. GSEA pathway enrichment analysis

For conducting GSEA analysis on the AHNAK2 gene, it is necessary to acquire expression data from publicly available databases like TCGA and arrange it in a descending order. Samples can be grouped into high-expression and low-expression groups using the median expression value as a threshold. The GSEA software can conduct pathway enrichment analysis, and various pathway collections such as KEGG, GO_BP, GO_CC, and GO_MF can be chosen as reference gene sets. After importing the grouping information and expression matrix file, GSEA analysis can be run with appropriate parameters. The enriched pathways can then be evaluated to investigate the biological functions and regulatory pathways associated with AHNAK2 in tumor development. Further analysis of biologically relevant pathways can reveal the mechanistic roles of AHNAK2 in tumor development.

2.15. Adhesion assay

For the cell-ECM adhesion assay, coat a 96-well plate with fibronectin at 37 °C for 1 h, wash twice with 0.1 % BSA in DMEM, block with 0.5 % BSA in DMEM at 37 °C for 60–120 min, seed cells, wash away unbound cells with PBS, add 100 μl medium with 10 % CCK-8, incubate at 37 °C for 3 h, and measure absorbance at 450 nm. For the cell-cell adhesion assay, grow a confluent cell layer to 70–80 %, rinse with Ca2+ and Mg2+-free PBS, detach cells with HBSS containing 1 mmol/l EDTA at 37 °C for 20 min, add 100 μl single-cell suspension (1×10^5 cells/ml) to the confluent layer, incubate at 37 °C for 0–120 min, wash unbound cells, and quantify adhesion as (N0-Nt)/N0 × 100, where Nt is the number of unbound cells and N0 is the initial cell number.

2.16. Western blot

Western blot analysis was conducted as previously described [23].

2.17. Gene ontology (GO) and Kyoto Encyclopedia of genes and genomes (KEGG) pathway enrichment analyses

GO and KEGG analysis was used to screen the co-expressed genes closely related to AHNAK2. Applying criteria of $|R| > 0.3$ for the absolute value of the correlation coefficient and $P < 0.05$, AHNAK2 co-expression genes were screened from PC cases in the cBioportal database. Then DAVID online tools (DAVID6.8 https://david.ncifcrf.gov/) were applied to GO and KEGG analysis. Additionally, the GO analysis encompassed three main categories: cellular component (CC), molecular function (MF), and biological process (BP). The differentially expressed genes were submitted to DAVID for analysis, and the outcomes were graphically presented using the "ggplot2″ R package.

2.18. Construction of co-expressed gene protein interaction network

We used the STRING database to create protein-protein interaction (PPI) networks based on co-expressed genes from the cBioPortal database. The resulting PPI networks were then visualized using Cytoscape software. Significant modules were identified using MCODE plugins. The top three modules were selected for enrichment analyses of the genes they contain using GO and KEGG.

2.19. Infiltrating immune cells analysis

The TIMER database was used to examine the expression patterns of AHNAK2 in PC. Furthermore, the relationship between AHNAK2 expression levels and the abundance of six unique infiltrating immune cell types, including B cells, macrophages, dendritic cells, $CD4^+$ T cells, $CD8^+$ T cells, and neutrophils, in the PC context were analyzed. Furthermore, this study examined the relationship between AHNAK2 and immune markers associated with dendritic cells (HLA-DRA, HLA-DPA1), the Th1 response (STAT1, IFN-γ), the TH22 pathway (AHR, CCR10), T cell depletion (GZMB, LAG3), natural killer cells (KIR2DL1, KIR2DL4, KIR3DL2), and $CD8^+$ T cells (CD8A). It is noteworthy that all correlation coefficients were adjusted according to tumor purity to ensure accurate interpretations.

The TCGA's PC samples were retrieved from the UCSC database using the link provided (https://xenabrowser.net/). From the dataset, expression data for the AHNAK2 gene was extracted and transformed using log2(x+0.001) conversion to ensure optimal suitability for analysis, and the gene expression profile relevant to PAAD was isolated and mapped to GeneSymbol for further investigation. This process was enabled through the use of the CIBERSORT deconvolution method, which is accessible via the IOBR R package (CIBERSORT: Robust enumeration of cell subsets from tissue expression profiles) [24]. The infiltration scores of 22 categories of immune cells for each patient in the AHNAK2 low and high expression groups were reassessed based on gene expression, including B cells naive, B cells memory, Plasma cells, T cells CD8, T cells CD4 naive, T cells CD4 memory resting, T cells CD4 memory activated, T cells follicular helper, T cells regulatory (Tregs), T cells gamma delta, NK cells resting, NK cells activated, Monocytes, Macrophages M0, Macrophages M1, Macrophages M2, Dendritic cells resting, Dendritic cells activated, Mast cells resting, Mast cells activated,

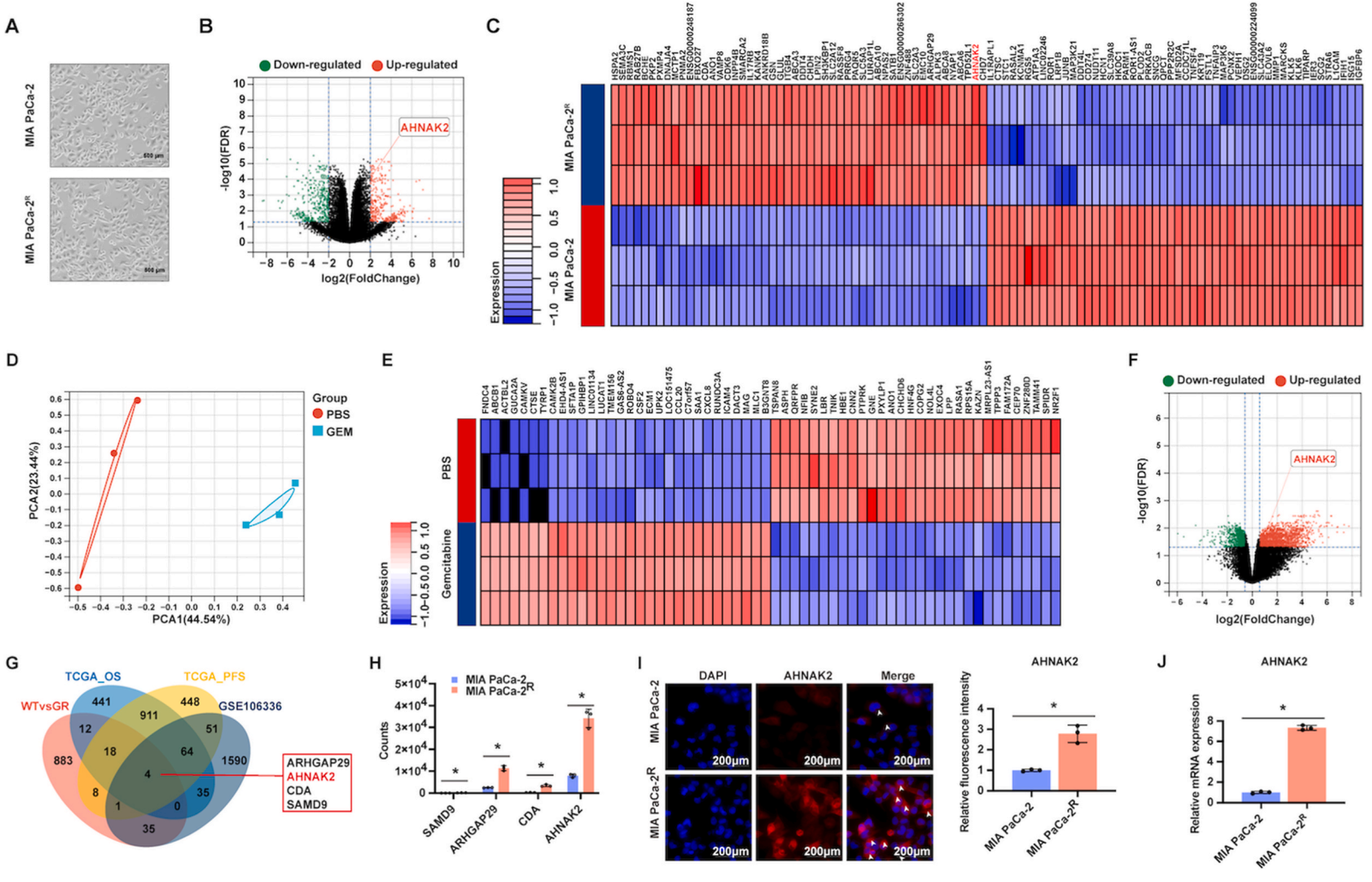

Fig. 1. AHNAK2 is associated with gemcitabine resistance and prognosis of pancreatic cancer. (A) Cell morphology of MIA PaCa-2 and MIA PaCa-2^{R}. (B) Volcano map of differentially expressed genes in transcript sequencing with |logFC| > 2 and $P < 0.05$. (C) Heatmap of top 100 differentially expressed genes in transcript sequencing with |logFC| > 2 and $P < 0.05$. (D) Principal component analysis of GSE106336. (E) Heatmap of top 50 differentially expressed genes in GSE106336 with |FoldChange| > 1.5, FDR <0.05. (F) Volcano map of differentially expressed genes in GSE106336 with |FoldChange| > 1.5 and FDR <0.05. (G) The Venn diagram showed the common genes among gene sets of the transcript sequencing, differentially expressed genes in GSE106336, OS-related genes, and PFS-related genes in the TCGA PAAD database. (H) The expression levels of four common differential genes (SAMD9, ARHGAP29, CDA, AHNAK2) in the transcriptome sequencing results were analyzed. (I) Immunofluorescence Analysis of AHNAK2 Expression in MIA PaCa-2 and MIA PaCa-2^{R}. White arrows indicate cytoplasm, and * indicates $P < 0.05$. (J) AHNAK2 mRNA expression of MIA PaCa-2 and MIA PaCa-2^{R} was evaluated by qRT-PCR.*$P < 0.05$.

Eosinophils, and Neutrophils.

2.20. Exploration of the correlation between AHNAK2, immune regulatory genes and immune checkpoint genes

Furthermore, utilizing the TIMER database, we investigated the correlation between AHNAK2 gene expression levels and the expression levels of immune regulatory genes, as well as the expression levels of immune checkpoint genes including both immune suppressive and immune stimulatory genes. We used Spearman correlation analysis for this assessment, and the correlation coefficients were adjusted based on tumor purity. This analysis enabled us to preliminarily investigate the potential involvement of the AHNAK2 gene in regulating tumor immunity.

2.21. Statistical analysis

This article employed multiple statistical methods to explore relationships between variables and differences between groups. The means of two or more groups were compared using the two-sample independent *t*-test for two groups and the one-way ANOVA for multiple groups. Spearman rank correlation analysis was employed to explore relationships between variables in cases of non-normally distributed data. Kaplan-Meier analysis was utilized to evaluate survival disparities among groups. In this study, statistical significance was defined as a *P*-value below 0.05.

3. Results

3.1. AHNAK2 is linked to both gemcitabine resistance and the prognosis of pancreatic cancer

As depicted in Fig. 1A, no observable differences were evident in terms of morphology and size between gemcitabine-treated MIA PaCa-2^R and their parental MIA PaCa-2 counterparts. Then MIA PaCa-2^R and MIA PaCa-2 cells were sent for transcriptome sequencing. DEGs were screened according to $|\log FC| > 2$ and $P < 0.05$. A volcanic diagram (Fig. 1B) shows 961 upregulated and 934 down-regulated genes. And the top 100 DEGs based on *P*-values were presented as a heat map (Fig. 1C). To further explore the differentially DEGs up-regulated in PC after gemcitabine treatment, the GSE106336 dataset was retrieved from the public GEO database and then analyzed. We screened for the up-regulated DEGs in PC cells after gemcitabine treatment according to the threshold of Fold Change >1.5 and FDR <0.05. The overall expression profile and heat map were shown in Fig. 1 D and E. FDR <0.05 was used as the threshold to screen DEGs, and 2609 DEGs were obtained. Compared with the parental cell line, 1780 genes were up-regulated, and 829 genes

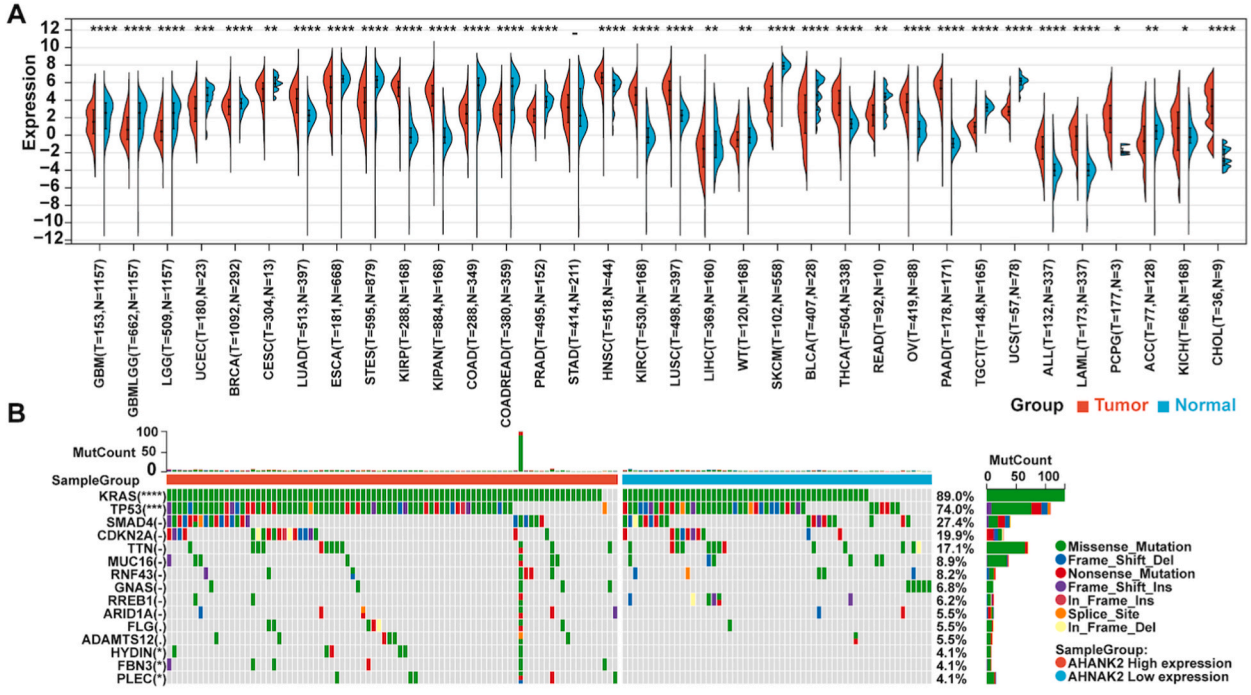

Fig. 2. Pan-cancer expression of AHNAK2 and its association with common tumor-mutated genes in pancreatic cancer. (A) The expression profiles of AHNAK2 across 34 distinct tumor tissues and their respective normal counterparts were extracted from the UCSC database. Significance levels were indicated as $*P < 0.05$, $**P < 0.01$, $***P < 0.001$, and $****P < 0.0001$. (B) Mutation landscape of top 15 genes in AHNAK2 high expression group and AHNAK2 low expression group.

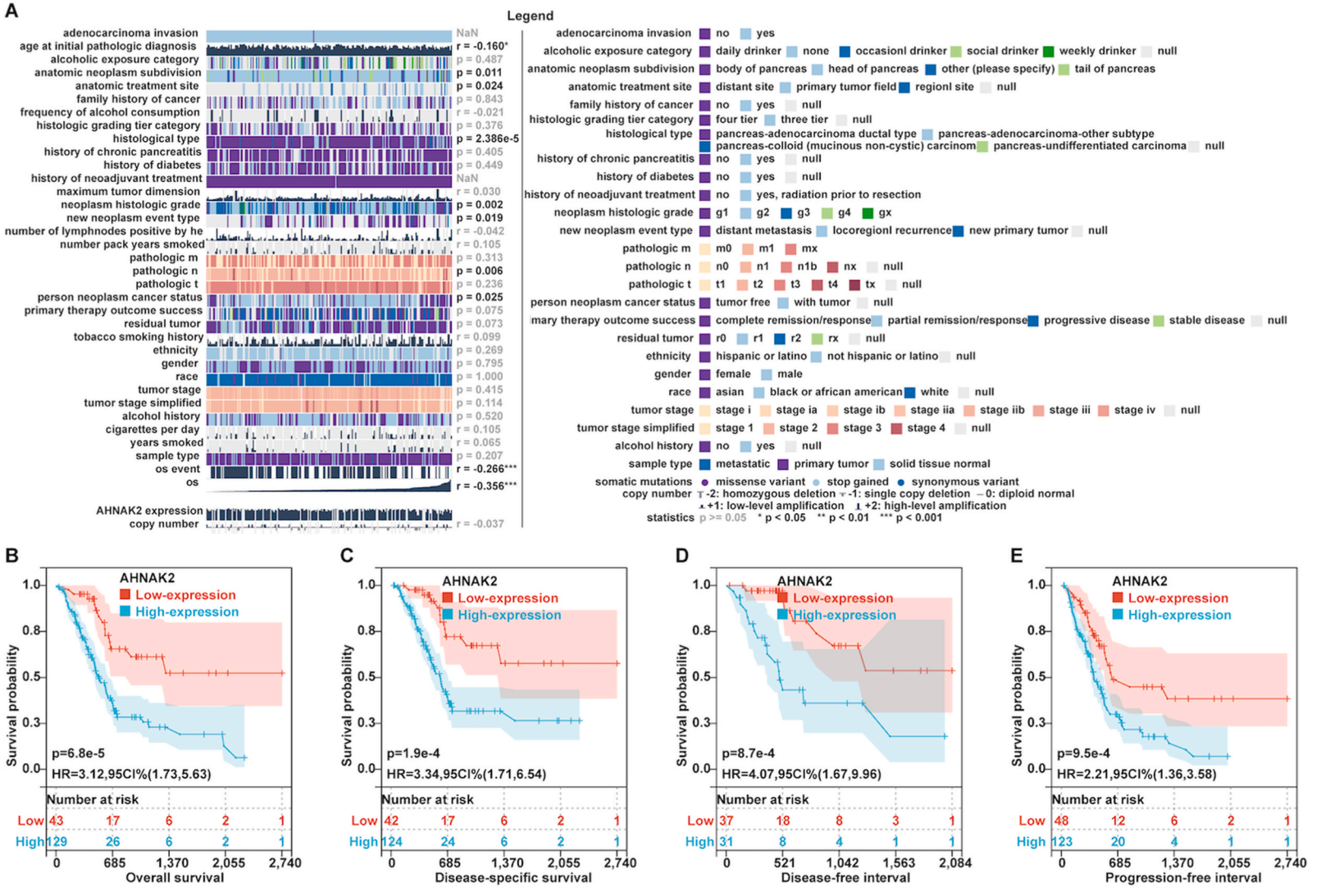

Fig. 3. Correlation of AHNAK2 expression with clinicopathological factors and survival prognosis of pancreatic cancer. (A) MEXPRESS-based correlation analysis between AHNAK2 expression and clinicopathological features of pancreatic cancer in TCGA database. Statistical significance is displayed in the middle column, and the quantitative data were tested using the Pearson correlation test, where a positive r suggests a positive correlation, and a negative number suggests a negative correlation. Qualitative data were analyzed using one-way ANOVA. *$P < 0.05$, **$P < 0.01$, ***$P < 0.001$. (B–E) Kaplan-Meier curves for AHNAK2 gene expression in pancreatic cancer cases: (B) Overall Survival (OS); (C) Disease-Specific Survival (DSS); (D) Disease-Free Interval (DFI); (E) Progression-Free Interval (PFI). Each curve represents the impact of AHNAK2 expression on survival outcomes. Statistical significance was assessed using the log-rank test. The shaded area indicated 95 % confidence interval (95 % CI).

were down-regulated in the gemcitabine-resistant cell lines and displayed as a volcano plot (Fig. 1F). In order to screen the genes associated with OS and PFS in PC, we performed a whole-gene survival analysis based on PAAD pancreatic cancer cases in the TCGA database. Relevant gene sets were screened according to HR > 1 and FDR <0.05. There were 1485 genes associated with OS, and 1505 genes associated with PFS overlapped with the two gene sets.

According to our transcriptome sequencing results, the analysis of up-regulated DEGs in GSE106336, and genes related to OS and PFS in TCGA-PAAD, the Venn diagram of the four gene sets was drawn and the intersection of the four gene sets was calculated. This intersection contained four differentially expressed genes, including AHNAK2, ARHGAP29, CDA, and SAMD9 (Fig. 1G). Out of these four genes, AHNAK2 exhibited the highest expression in gemcitabine-resistant cells, as discerned from transcriptome sequencing data (Fig. 1H). Therefore, the AHNAK2 gene was selected for further investigation in this study. Immunofluorescence analysis demonstrated elevated AHNAK2 expression in gemcitabine-resistant PC cell lines (Fig. 1I, $P < 0.05$). Further, qRT-PCR results confirmed that AHNKA2 was up-regulated in gemcitabine-resistant PC cell lines (Fig. 1J, $P < 0.05$).

3.2. Pan-cancer expression level of AHNAK2 and its association with mutated genes in pancreatic cancer

To explore the clinical significance of AHNAK2, we acquired a standardized pan-cancer dataset from the UCSC database. We then extracted AHNAK2 gene expression data from each sample included in the dataset. For each tumor type, we computed the expression differences between normal and tumor samples using R software (version 3.6.4). The distribution of AHNAK2 gene expression in the above 34 tumor tissues was plotted. The abscissa represents different cancer types, and the ordinate represents the AHNAK2 expression. AHNAK2 exhibited significant up-regulation in 13 different tumor types (KIRP, KIPAN, HNSC, KIRC, LUAD, LUSC, THCA, OV, PAAD, CHOL, ALL, LAML, PCPG), including the pancreatic cancer TCGA-PAAD. And AHNAK2 was downregulated in 19 tumors (GBMLGG, SKCM, LGG, LIHC, TGCT, PRADT, UCEC, READ, BLCA, GBM, COAD, CESC, STES, COADREAD, ESCA, BRCA, UCS, WT, ACC.) (Fig. 2A). Furthermore, for the TCGA-PAAD database, 81.5 % of the 178 samples contains top 15 mutations (including KRAS, TP53, SMAD4, CDKN2A, TTN, MUC16, RNF43, GNAS, RREB1, ARID1A, FLG, ADAMTS12, HYDIN, FBN3, and PLEC) and were used for further analysis The samples were stratified into high and low expression groups based on AHNAK2 expression levels. The chi-square test was utilized to assess variations in gene mutation frequency across distinct AHNAK2 expression levels, and the results of gene mutation differences were presented in the gene mutation landscape. In the AHNAK2 high expression group, KRAS and TP53 mutation frequencies were notably elevated (Fig. 2B). This observation underscores the close association between AHNAK2 and oncogene mutations in PC.

3.3. AHNAK2 demonstrates a correlation with the clinicopathological characteristics of pancreatic cancer

The MEXPRESS website was employed to scrutinize the interplay between AHNAK2 gene expression levels and clinical factors

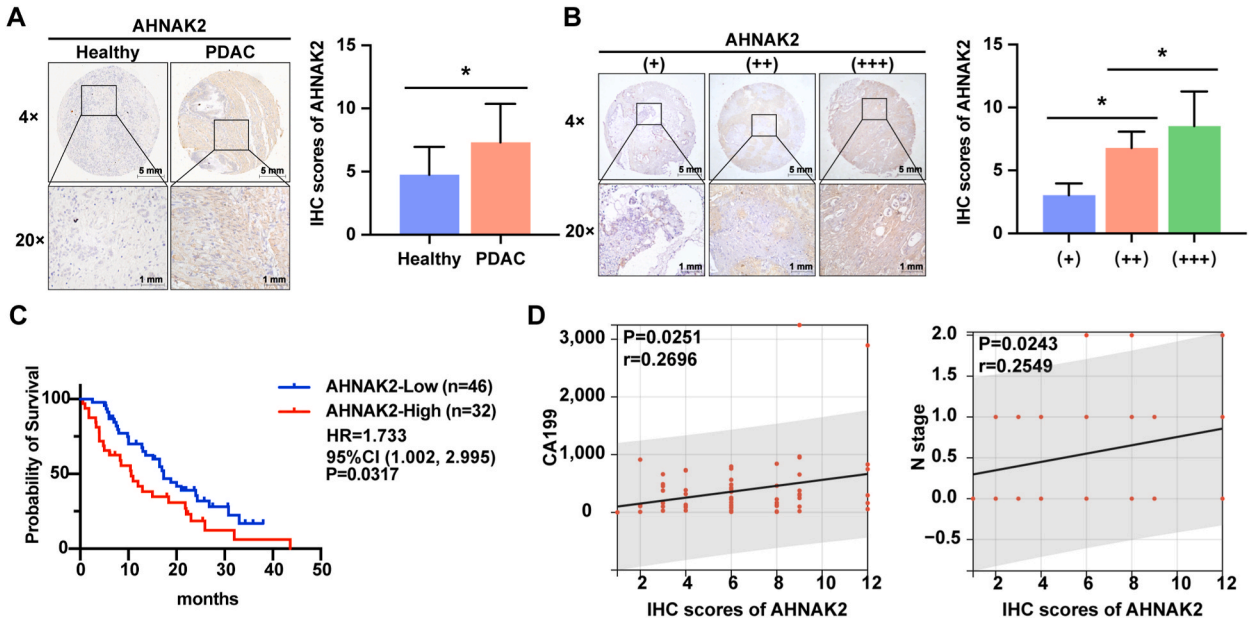

Fig. 4. The correlation of ANHAK2 expression with survival prognosis and clinicopathological characteristics of pancreatic cancer was verified in human specimens. (A–B) Immunohistochemical staining images depict AHNAK2 gene expression in pancreatic cancer tissue microarray sections. Panels (A) and (B) visually represent the expression patterns within cancerous tissues. (C) Kaplan-Meier survival curve analysis was performed using immunohistochemical scoring data to explore the relationship between AHNAK2 gene expression levels and patient prognosis. The plot illustrates the potential impact of AHNAK2 expression on survival outcomes. (D) Correlation analysis of AHNAK2 expression level with CA199 and N stage.

within PC. This analysis aimed to provide an initial understanding of the potential correlation between the AHNAK2 gene and the clinicopathological attributes of PC. As depicted in Fig. 3A, AHNAK2 gene expression levels exhibited variations across distinct histological types of PC ($P < 0.001$), different Grade stages (G1, G2, G3, G4, $P = 0.002$), and diverse N stages (Stage 1, Stage 2, Stage 3, Stage 4, $P = 0.006$). Moreover, AHNAK2 gene expression levels exhibited a negative correlation with patient survival ($r = -0.266$, $P < 0.001$) and OS ($r = -0.356$, $P < 0.001$). To strengthen the validation of AHNAK2's prognostic significance in PC patients, we employed the log-rank method to analyze the TCGA pancreatic cancer dataset. The findings demonstrated a correlation between high AHNAK2 expression and unfavorable OS (HR = 3.12, $P < 0.05$), disease-specific survival (DSS, HR = 3.34, $P < 0.05$), disease-free interval (DFI, HR = 4.07, $P < 0.05$), progression-free interval (PFI, HR = 2.21, $P < 0.05$) (Fig. 3B–E).

3.4. AHNAK2 was up-regulated in pancreatic cancer tissue microarray

Each microarray tissue was scored according to the immunohistochemical scoring criteria. Immunohistochemical analysis substantiated the heightened expression of AHNAK2 in PC tissues as opposed to normal tissues (Fig. 4A–B, $P < 0.05$). Simultaneously, Kaplan-Meier curves were constructed to depict the relationship between AHNAK2 expression levels and OS in diverse PC patients (Fig. 4C). The outcomes highlighted that AHNAK2 expression levels exhibited a negative correlation with OS and were identified as a risk factor for PC (HR = 1.733, $P = 0.0317$). Notably, the AHNAK2 high expression group displayed a median survival time of 10.6 months, in contrast to 17.3 months for the AHNAK2 low expression group. Moreover, AHNAK2 expression levels demonstrated a positive correlation with serum CA199 levels ($r = 0.2696$, $P = 0.0251$) and N stage ($r = 0.2549$, $P = 0.0243$) (Fig. 4D). Furthermore, based on the immunohistochemical AHNAK2 score, patients were classified into a high-expression group (n = 32) and a low-expression group (n = 46). Subsequent analysis of clinicopathological characteristics unveiled statistically significant differences in clinical stage, N stage, and serum CA199 expression levels between these two groups (Table 1).

3.5. Knockdown of AHNAK2 inhibited cell proliferation and gemcitabine resistance in PC

We conducted AHNAK2 knockdown experiments on MIA PaCa-2^R cells using siRNA. The transfection efficacy was confirmed via qRT-PCR and immunofluorescence staining (Fig. 5A and B). Due to the large molecular weight of AHNAK2, we were unable to use Western blotting to detect AHNAK2 protein expression. Additionally, we confirmed that AHNAK2 influences pancreatic cancer cell proliferation through CCK-8 assays (Fig. 5C). We then determined the IC50 of gemcitabine in MIA PaCa-2^R cells following AHNAK2 knockdown. The results (Fig. 5D) indicated that the gemcitabine IC50 was 1394 nM in the control group, 145.9 nM in the siAHNAK2#1 group, and 183 nM in the siAHNAK2#2 group. These findings suggest that knocking down AHNAK2 expression in drug-resistant cells

Table 1
Relationship between AHNAK2 expression level and clinicopathological features in pancreatic cancer tissue microarray.

Clinical parameters	All cases	AHNAK2 expression		*P*-Value
		Low	High	
Age				0.3166
≤60	29	15	14	
>60	49	31	18	
Gender				0.12
Male	43	22	21	
Female	35	24	11	
Stage				0.0308[a]
Stage I		18	5	
Stage II		13	11	
Stage III		6	5	
Stage IV		9	11	
T Classificaiton				0.221
T1	7	5	2	
T2	28	19	9	
T3	26	13	13	
T4	17	9	8	
N Classification				0.0393[a]
N0	37	26	11	
N1	37	19	18	
N2	4	1	3	
M Classification				0.2881
M0	59	37	22	
M1	19	9	10	
AFP (ng/ml)	75	2.538 ± 0.2518	2.267 ± 0.3306	0.5089
CEA (ng/ml)	76	8.021 ± 4.010	7.359 ± 2.163	0.8983
CA125 (U/ml)	68	39.02 ± 13.28	68.46 ± 30.90	0.3345
CA199 (U/ml)	69	258.9 ± 36.33	731.7 ± 215.4	0.0459[a]

AFP, CEA, CA125, CA199 were presented by MEAN ± SEM.
[a] $P < 0.05$.

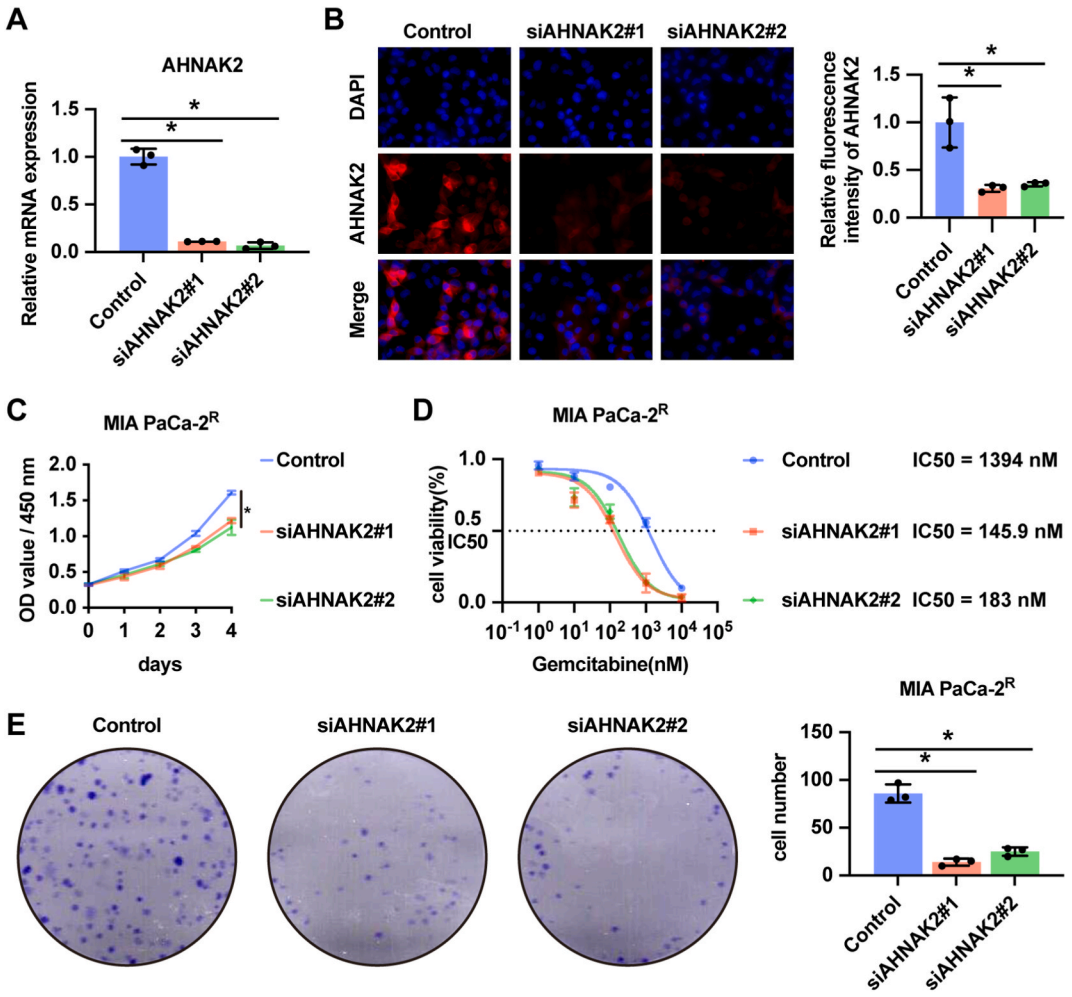

Fig. 5. Down-regulation of ANNAK2 expression inhibits pancreatic cancer's proliferation and drug resistance. (A) siRNA was used to knock down the expression of AHNAK2 in MIA PaCa-2^R and qRT-PCR was performed to validate the AHNAK2 mRNA expression. (B) Cellular immunofluorescence was used to confirm the AHNAK2 expression. *$P < 0.05$. (C) CCK-8 was used to detect the cell proliferation of MIA PaCa-2^R. *$P < 0.05$. (D) IC50 of gemcitabine to MIA PaCa-2^R was detected using CCK-8. (E) Plate colony formation assay was used to detect the ability of colony formation in MIA PaCa-2^R. *$P < 0.05$.

increases gemcitabine toxicity. Furthermore, AHNAK2 knockdown inhibited the colony formation ability of drug-resistant cells (Fig. 5E).

3.6. GSEA pathway enrichment analysis of AHNAK2 single gene

To further explore the changes in molecular pathways caused by AHNAK2, we performed single gene GSEA pathway enrichment analysis for AHNAK2 in GO_BP, GO_CC, GO_MF and KEGG pathways based on the TCGA-PAAD database (Fig. 6A). GSEA enrichment results of GO_BP gene set showed that high expression of AHNAK2 group was mainly enriched in keratinocyte proliferation, embryonic skeletal system development, regulation of epidermal development, spindle organization pathway, NAD metabolism pathway (FDR <0.05). GSEA enrichment results of the GO_CC gene set indicated that high expression of AHNAK2 group was mainly enriched in cell components such as desmosome, apical junction complex, cleavage furnaces, aggrecan, and ankyrin (FDR <0.05). GSEA enrichment results of the GO_MF gene set showed that high expression of AHNAK2 group was mainly enriched in cadherin binding, cell-cell adhesion mediator, cell adhesion molecule binding, cell adhesion mediator activity, and cadherin binding involved in intercellular adhesion (FDR <0.05). GSEA enrichment results of KEGG pathways high expression of AHNAK2 group was mainly enriched in the pentose phosphate pathway, p53 signaling pathway, axon guidance, and ECM-receptor interaction (FDR <0.05).

We knocked down AHNAK2 expression in the drug-resistant cell line MIA PaCa-2^R with siRNA and explored the effects of AHNAK2 knockdown on cell-cell and cell-ECM adhesion by adhesion assay. The results showed that knockdown of AHNAK2 enhanced cell-ECM adhesion and inhibited cell-cell adhesion (Fig. 6B, $P < 0.05$). Further, we detected the KRAS and p53 protein expression and mRNA

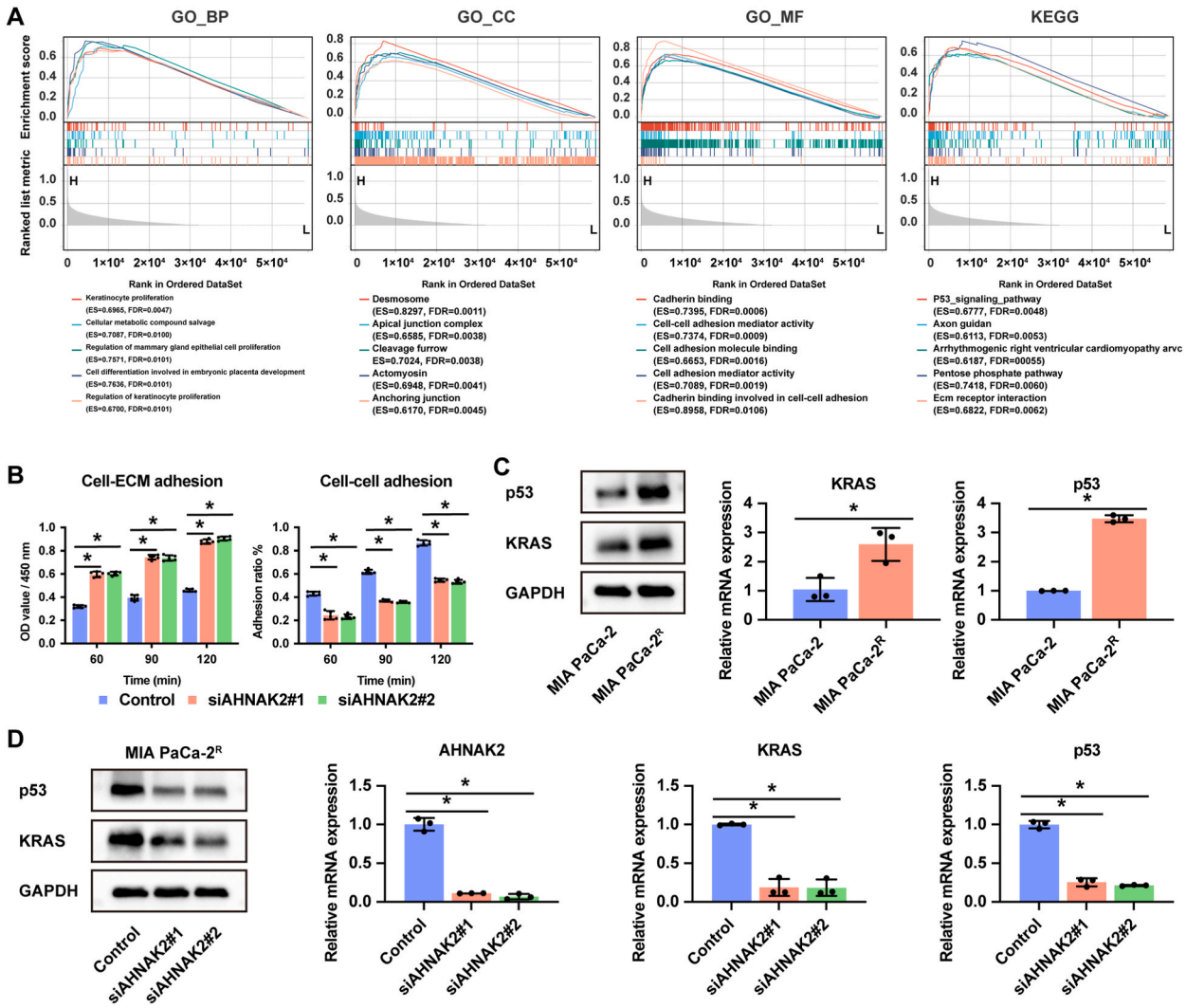

Fig. 6. AHNAK2 correlated with cell-cell and cell-ECM adhesion and KRAS/p53 signaling pathway. (A) GSEA was employed to investigate pathway enrichment associated with AHNAK2 in the TCGA PAAD database. This analysis sheds light on potential biological pathways influenced by AHNAK2 gene expression. (B)Adhesion assay was used to detect cell-ECM adhesion and cell-cell adhesion of pancreatic cancer cells after knocking down AHNAK2 expression using siRNA. $*P < 0.05$. (C) Western blot and qRT-PCR were used to evaluate the expression of KRAS and p53 in MIA PaCa-2 and MIA PaCa-2^R. The original image is shown in Fig.S1-3. (D) Western blot was used to evaluate the protein expression of KRAS and p53 after siRNA-mediated AHNAK2 knocking down in MIA PaCa-2^R. qRT-PCR was used to evaluate the mRNA expression of KRAS, p53, and AHNAK2 after siRNA-mediated AHNAK2 knocking down in MIA PaCa-2^R. GAPDH is the internal control. The original image is shown in Fig.S4-6.

expression of MIA PaCa-2 and MIA PaCa-2^R. The results showed that KRAS and p53 expression were upregulated in drug-resistant cells (Fig. 6C). After the knocking down of AHNAK2 in MIA PaCa-2^R, the KRAS and p53 expression were subsequently downregulated (Fig. 6D).

3.7. Results of genes enrichment analysis for AHNAK2 co-expressed genes

To identify co-expressed genes strongly associated with AHNAK2, we filtered 955 genes that exhibited a positive co-expression relationship and a significance level ($P < 0.05$). This selection was conducted using the Co-expression module within the cBioportal database, focusing on pancreatic cancer cases. 955 genes were imported to DAVID online tools. Gene biological process (BP), cell component (CC) and molecular function (MF) changes, gene ontology (GO) analysis of co-expressed gene sets was performed. As shown in Fig. 7, in the BP enrichment results, AHNAK2 co-expressed genes were significantly enriched in "signal transduction, cell adhesion, transmembrane receptor protein tyrosine kinase signaling pathway, cell-cell adhesion, inflammatory response" and other biological processes. In terms of CC enrichment, AHNAK2 co-expressed genes were mainly enriched in "plasma membrane, integral component of plasma membrane, cell surface, extracellular exosome, receptor complex" and other cellular components. In the MF rich

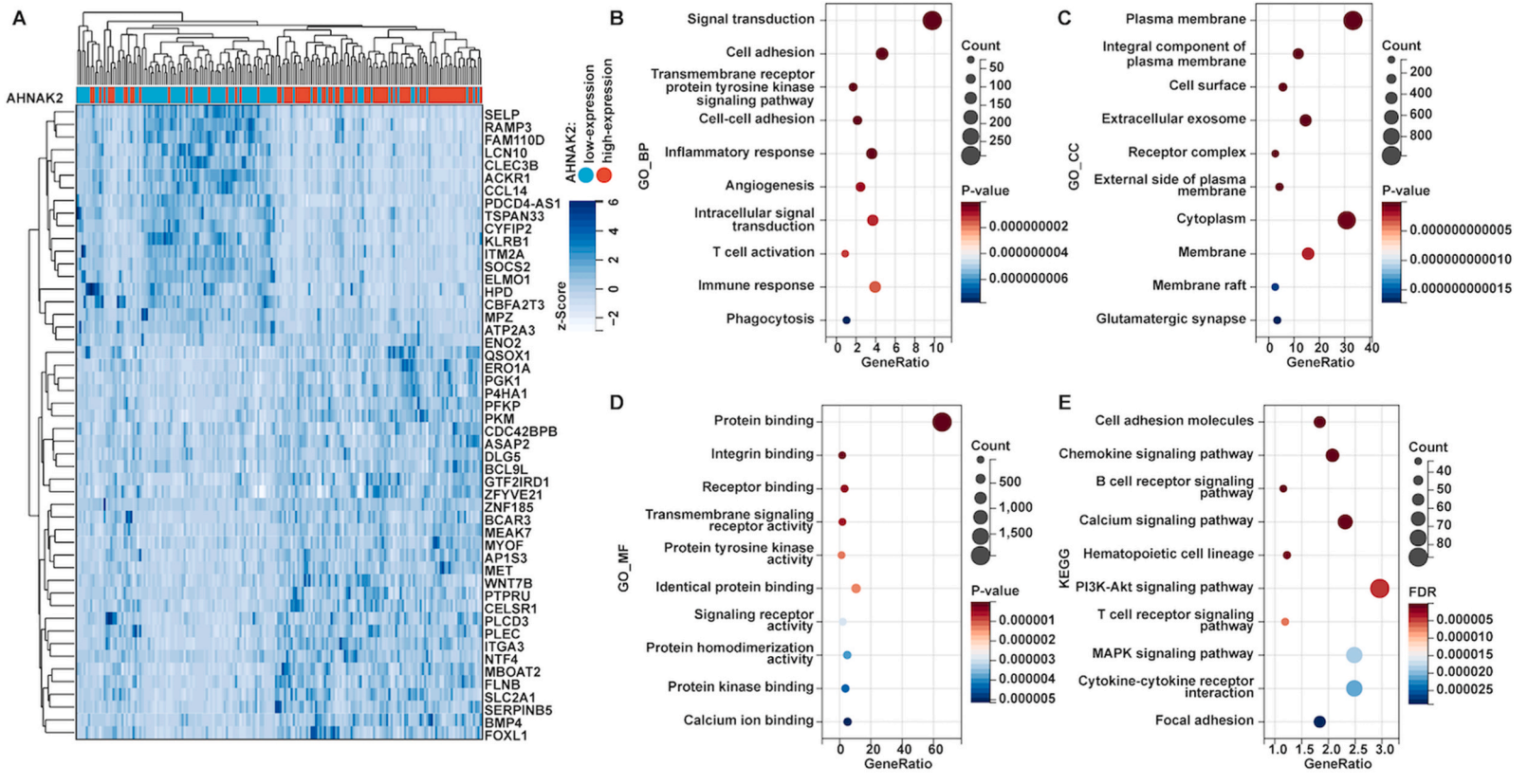

Fig. 7. AHNAK2 Co-expressed genes enrichment analysis: Go and KEGG pathways. (A) Top 50 Heatmap of positively correlated genes. (B) Go biological process (GO_BP) enrichment. (C) Go cellular component (GO_CC) enrichment. (D) GO molecular function (GO_MF) enrichment. (E) KEGG Pathway enrichment.

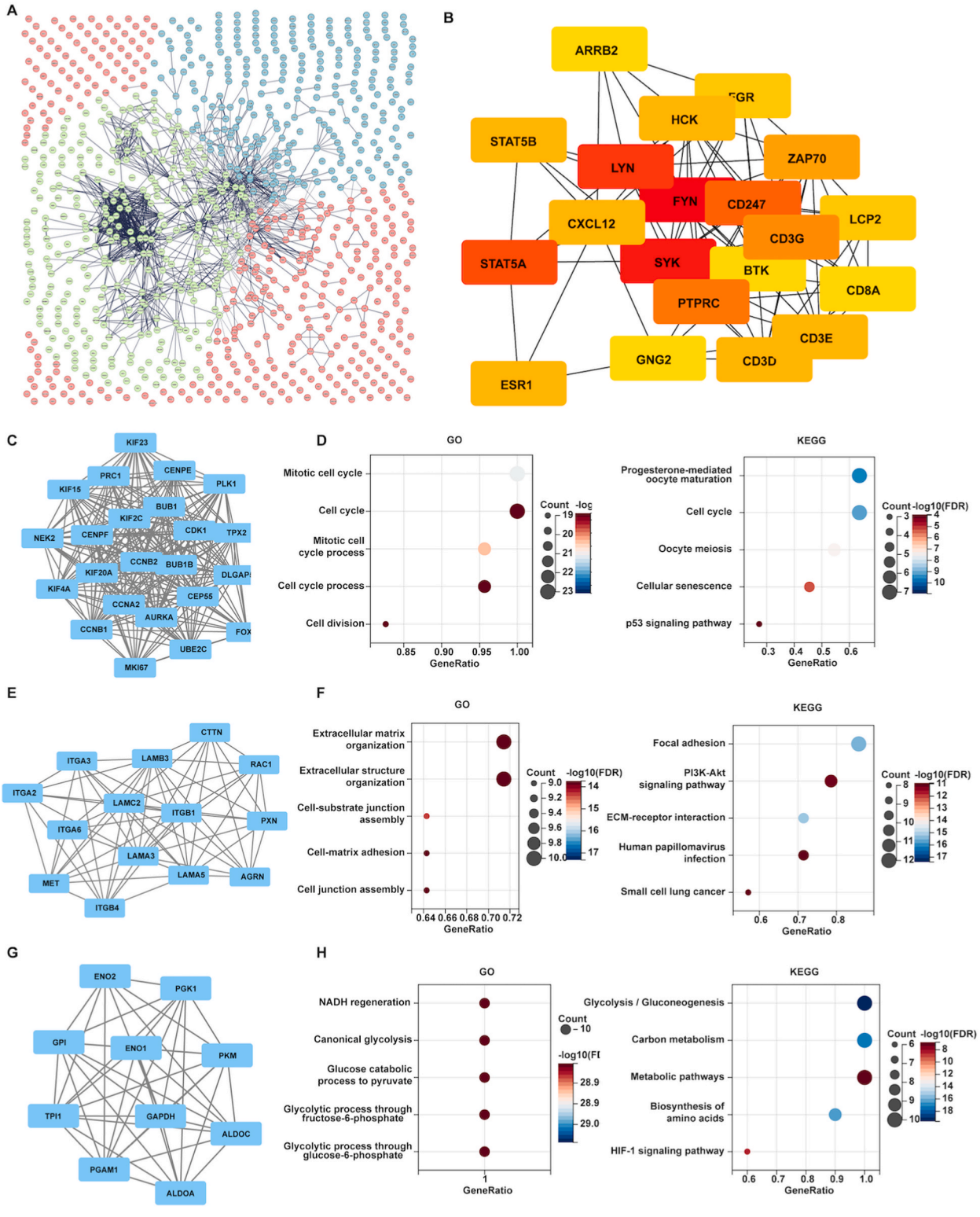

(caption on next page)

Fig. 8. Construction of PPI protein interaction network and identification of key modules. (A) The protein-protein interaction network of AHNAK2 co-expression positive related genes was constructed by the STRING database. (B) Essential hub genes were identified by the Cytocubba plug-in of Cytoscape software, 224 hub genes were identified according to degree >3, and the top 20 genes were extracted for visualization. Identification of key modules of protein interaction network of AHNAK2 co-expressed genes and enrichment analysis of GO and KEGG. Three key modules were identified, and the scores were 21.727(C), 10.462(E), and 9.333(G), respectively. D, F, and H show the corresponding GO and KEGG pathway enrichment analysis.

set, "protein binding, integrin binding, receptor binding, transmembrane signaling receptor activity, protein tyrosine kinase activity" was the main molecular function. The KEGG pathway enrichment analysis unveiled significant enrichment of AHNAK2 co-expressed genes in pathways such as cell adhesion molecules, chemokine signaling pathway, B cell receptor signaling pathway, calcium ion signaling pathway, hematopoietic cell lineage, PI3K-AKT signaling pathway, T cell receptor signaling pathway, and more.

3.8. Protein-protein interaction and key module construction of AHNAK2 positively co-expression proteins

The construction of the protein-protein interaction (PPI) network involved inputting AHNAK2-positive co-expression genes by using the STRING website tool, followed by visualization using the Cytoscape software. As shown in Fig. 8A, after hiding the nodeless network, the network contains 924 nodes and 1349 edges. The "degree" algorithm within CytoHubba was utilized to calculate the connectivity edges (degree) among co-expressed genes. This process led to the identification of the top 20 genes based on their degree as Hub genes (Fig. 8B). In addition, the utilization of the MCODE tool within the Cytoscape software facilitated the computation of pivotal modules. The top three key modules were found, and GO and KEGG enrichment analyses on these three key modules were performed. Concerning key module one (Fig. 8C and D), it actively engaged in important biological processes in the context of PC, encompassing the regulation of cell cycle, cell division, oocyte development, cell senescence, and p53 signaling pathway. As for the genes comprising key module two (Fig. 8E and F), they demonstrate intimate associations with the structural and organizational control of the extracellular matrix. Among them, the processes include the regulation of extracellular matrix organization and extracellular structure organization, the binding between cells and matrix, and the connection between cells. The observation implies that these genes might hold a crucial function in governing interactions between cells and tissues within the extracellular matrix. KEGG results suggest that module two genes are involved in cell adhesion, cell signaling, and extracellular matrix interaction. According to GO enrichment analysis outcomes, the genes within key module three (Fig. 8G and H) participate in processes like NADH regeneration, classical glycolysis, catabolism of glucose through pyruvate, glycolysis through fructose-6-phosphate, and glycolysis through glucose-6-phosphate. Based on the results of the KEGG enrichment analysis, the module genes were implicated in the regulation of the glycolysis/gluconeogenesis pathway, carbon metabolism, metabolic pathway, amino acid synthesis, and HIF-1 signaling pathway. These results mentioned above suggest that genes in key modules are involved in cellular energy metabolism, carbon metabolism, substance synthesis, and signaling pathways related to cellular response under hypoxic conditions.

Since these three key modules consisted of AHNAK2 co-expressed genes, it underscores the importance of AHNAK2 in PC. AHNAK2 gene might play a role in regulating the PC biological process by interacting with key module genes. These biological processes involve cell cycle regulation, cell division, cell senescence, p53 signaling pathway, organization and structure regulation of extracellular matrix, cell adhesion, cell signaling, glycolysis, glucose metabolism, carbon metabolism, amino acid synthesis, and cell response under hypoxic conditions. These results further underscore the pivotal significance of AHNAK2 in PC development and provide important clues for further research and utilization of AHNAK2's potential role in PC treatment.

3.9. Involvement of AHNAK2 in immune infiltration in pancreatic cancer

Based on a 22-category score measuring immune cell infiltration, the results showed (Fig. 9A) that in pancreatic cancer, the immune cell types exhibiting escalated infiltration score in the AHNAK2 high-expression group as opposed to the AHNAK2 low-expression group encompassed T cells regulatory (Treg), Macrophages M0, Macrophages M2, with statistically significant disparities. In tissues with high AHNAK2 expression, the cell types showing reduced immune cell infiltration scores included B cells naive, B cells memory, T cells CD8, and T cells CD4 naive. In summary, the AHNAK2 gene expression in PC demonstrates a strong correlation with the B cell humoral immunity pathway, cellular immunity pathway, macrophage polarization, and other immune processes. Further, we performed immunohistochemistry staining of CD68 for macrophages and CD20 for B cells in AHNAK2 low and high expression tissue of pancreatic cancer. Percent positivity was determined using HALO software (Indica Labs, Inc). The results showed that CD68 and CD20 were significantly upregulated in the AHNAK2 high expression group (Fig. 9B).

The TIMER database was utilized to investigate the relationship between the AHNAK2 gene and immune infiltration in pancreatic cancer patients. The results revealed significant associations between AHNAK2 gene expression and immune cell types. Specifically, the expression of AHNAK2 was positively correlated with $CD8^+$ T cells ($r = 0.154$, $P = 0.0448$) and dendritic cells ($r = 0.166$, $P = 0.0304$), while it exhibited a negative correlation with $CD4^+$ T cells ($r = -0.178$, $P = 0.0209$). Notably, AHNAK2 expression was positively correlated with $CD8^+$ T cells immune infiltration, which is inconsistent with Fig. 8A results and might be caused by different algorithms and gene signatures. The above results (Fig. 9C) suggested that AHNAK2 expression increased alongside the reduction of $CD4^+$ T cells proportion, implying its potential involvement in fostering tumor initiation and progression within the tumor immune microenvironment.

The results (Fig. 9D and Table S.1) indicated that the AHNAK2 expression displayed a negative correlation with CD8A ($r = -0.212$,

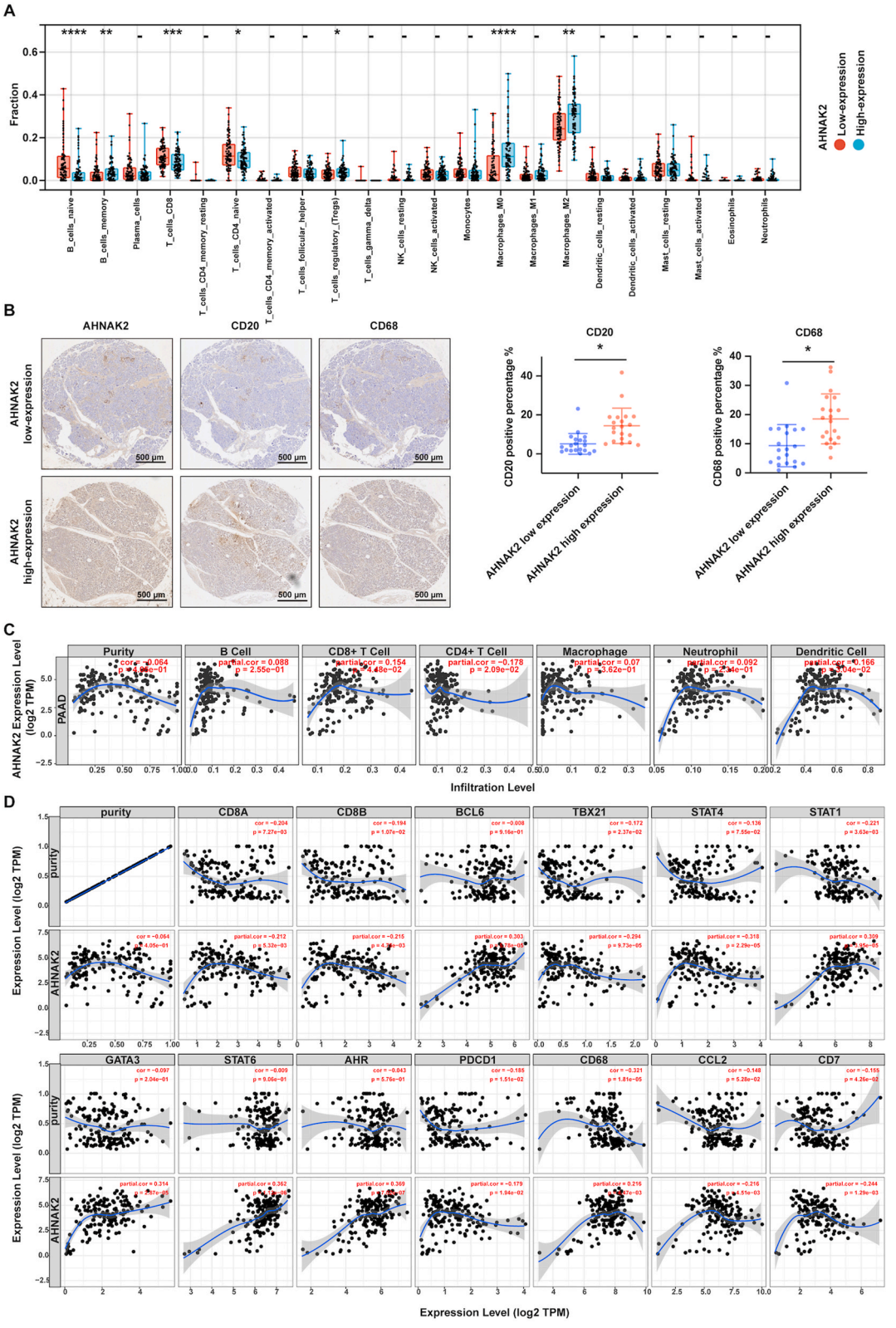

(caption on next page)

Fig. 9. AHNAK2 expression is associated with immune cell infiltration in pancreatic cancer. (A) In the TCGA database, the scores of 22 types of immune cell infiltration in pancreatic cancer patients with low and high AHNAK2 expression were, respectively. (B) Immunohistochemical staining analysis of CD20 and CD68 of AHNAK2 low and high expression tissue. (C) TIMER database was used to analyze the correlation between AHNAK2 gene expression level and immune cell score. (D) Furthermore, the TIMER database analyzed the correlation between AHNAK2 gene expression level and immune cell marker genes.

$P < 0.01$) and CD8B ($r = -0.215$, $P < 0.01$) of CD8+T cells, and a positive correlation with BCL6 of Tfh cells ($r = 0.303$, $P < 0.01$). AHNAK2 exhibited a negative correlation with TBX21 ($r = -0.294$, $P < 0.01$) and STAT4 ($r = -0.318$, $P < 0.01$) while displaying a positive correlation with STAT1 ($r = 0.309$, $P < 0.01$) in Th1 cells. AHNAK2 exhibited a positive correlation with GATA3 ($r = 0.314$, $P < 0.01$) and STAT6 ($r = 0.362$, $P < 0.01$) in Th2 cells, as well as with AHR of Th22 cells ($r = 0.369$, $P < 0.0001$). Conversely, AHNAK2 displayed a negative correlation with PDCD1 in T cell exhaustion ($r = -0.179$, $P < 0.05$). A positive correlation was observed with macrophage CD68 ($r = 0.216$, $P < 0.01$). However, a negative correlation was found between CCL2 in TAMs ($r = -0.216$, $P < 0.01$) as well as CD7 in NK cells ($r = -0.244$, $P < 0.01$). These results propose the potential influence of AHNAK2 on the PC tumor microenvironment through immune infiltration regulation, thereby promoting PC progression.

3.10. AHNAK2 was associated with immunomodulatory genes in pancreatic cancer

The TIMER database was employed to investigate the relationship between AHNAK2 and immunomodulatory genes, encompassing categories such as chemokines, receptors, major histocompatibility complex (MHC) genes, inhibitors, and stimulators. As shown in Table S.2, according to $|r| > 0.3$ and $P < 0.05$, AHNAK2 gene expression was negatively correlated with CCL14 ($r = -0.397$, $P < 0.01$) and CCL16 ($r = -0.354$, $P < 0.01$). AHNAK2 gene expression displayed a positive correlation with the MHC marker TAP ($r = 0.336$, $P < 0.01$) and the immunosuppressive gene TGFB1 ($r = 0.335$, $P < 0.01$), while negatively associated with immunosuppressive gene CD160 ($r = -0.318$, $P < 0.01$). Furthermore, AHNAK2 gene expression exhibited significantly positive correlations with immunomodulator stimulator genes, including NT5E ($r = 0.480$, $P < 0.01$), CD276 ($r = 0.409$, $P < 0.01$), RAET1E ($r = 0.340$, $P < 0.01$), TNFSF9 ($r = 0.426$, $P < 0.01$), PVR ($r = 0.305$, $P < 0.01$), ULBP1 ($r = 0.329$, $P < 0.01$), TNFSF4 ($r = 0.337$, $P < 0.01$), CD70 ($r = 0.326$, $P < 0.01$). These findings suggest a close association between AHNAK2 and immunomodulatory genes, indicating its potential role as a pivotal immunomodulatory target in PC progression.

3.11. AHNAK2 was correlated with immune checkpoint genes in pancreatic cancer

The efficacy of immunotherapy for PC is influenced by the degree of immune cell infiltration. To further investigate the potential role of AHNAK2 in the context of immunotherapy, we continue to explore the TIMER database to analyze the association of AHNAK2 with immune checkpoint genes, including immune checkpoint stimulating and inhibiting molecules according to $|r| > 0.3$ and $P < 0.05$. The findings presented in Fig. 10 and Table S.3 indicate that AHNAK2 expression levels exhibited positive correlations with immune checkpoint inhibitory molecules, namely CD276 ($r = 0.409$, $P < 0.01$), TGFB1 ($r = 0.335$, $P < 0.01$), and VEGFA ($r = 0.502$, $P < 0.01$). Conversely, AHNAK2 expression showed a negative correlation with the immune checkpoint inhibitor ARG1 ($r = -0.302$, $P < 0.01$). Furthermore, AHNAK2 gene expression displayed positive associations with IL1A ($r = 0.355$), TNFSF9 ($r = 0.426$), TNFSF4 ($r = 0.337$), CD70 ($r = 0.326$), and HMGB1 ($r = 0.349$). In contrast, it exhibited a negative association with SELP ($r = -0.326$). These findings offer additional substantiation that AHNAK2 is intricately linked to immune checkpoint genes in the context of pancreatic cancer. This reinforces the potential significance of AHNAK2 in the landscape of pancreatic cancer immunotherapy.

4. Discussion

Chemotherapy is still the primary clinical approach to enhance the lifespan of patients diagnosed with PC. At present, most first-line chemotherapy regimens include gemcitabine, but the resistance to gemcitabine chemotherapy has become the bottleneck of clinical treatment. For this research, we focused on identifying genes related to gemcitabine resistance by analyzing differentially expressed genes and conducting transcriptome sequencing and bioinformatics analysis on gemcitabine-resistant PC cells. Through this investigation, we discovered the AHNAK2 gene, which is closely related to gemcitabine resistance. To further validate the diagnostic and prognostic value of AHNAK2, the research conducted experiments using PC tissue microarray. Moreover, we utilized public databases to explore the role of AHNAK2 in tumor immune infiltration of PC. Remarkably, this study presents the first evidence linking AHNAK2 with gemcitabine resistance in PC and suggests that immune infiltration was a probable mechanism of AHNAK2 regulating gemcitabine resistance.

AHNAK2 gene is in 14q32 (band 2, region 3 of the long arm of chromosome 14), which was first reported in 2004. It is an oncogene found in recent years and closely related to a variety of malignant tumors derived from epithelial cells [25,26]. We acquired the pan-cancer dataset, which was harmonized and standardized, from the UCSC database. Our investigation revealed a noteworthy up-regulation of AHNAK2 in 13 distinct tumor types, comprising pancreatic ductal adenocarcinoma, lung adenocarcinoma, and renal clear cell carcinoma. These findings corroborated existing literature. AHNAK2, a protein of 616 kDa, exhibits limited understanding regarding its specific involvement in cancer mechanisms. In CCRCC, AHNAK2 is essential for hypoxia-induced EMT, which is mediated by HIF-1α. When AHNAK2 is suppressed, tumor migration is significantly inhibited. In addition, the suppression of AHNAK2 also impedes the synthesis of fatty acids and lipids, ultimately leading to the inhibition of tumor proliferation [27]. In uveal melanoma,

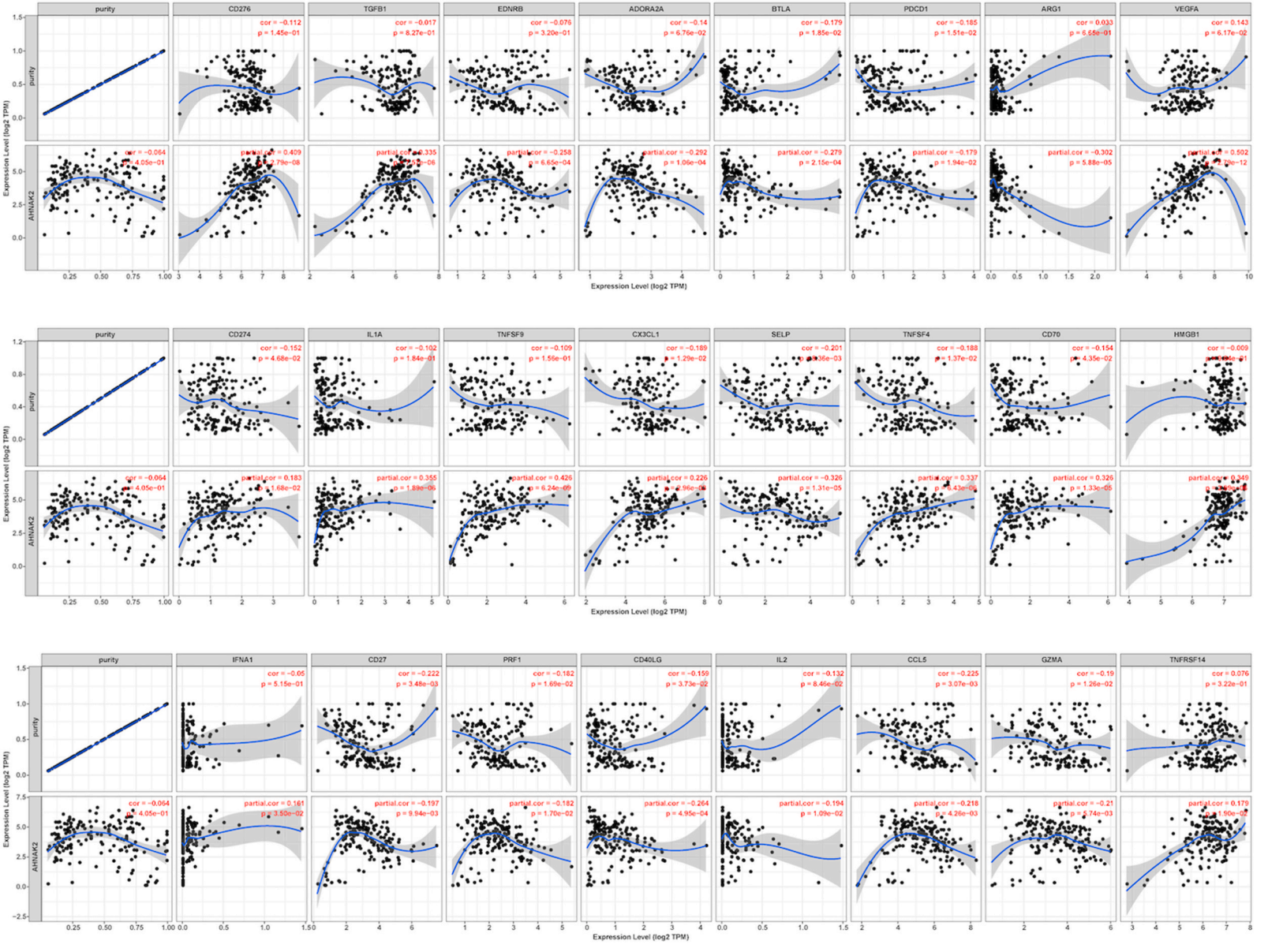

Fig. 10. AHNAK2 expression is correlated with immune checkpoint gene expression in pancreatic cancer. Based on the TIMER database, the correlation between AHNAK2 and immune checkpoint genes in pancreatic cancer was analyzed.

AHNAK2 up-regulates PI3K/AKT expression [28]. AHNAK2 induces activation of the TGF-β/Smad3 pathway in lung adenocarcinoma through the enhanced expression of *p*-Smad3 [29]. In thyroid cancer, AHNAK2 promotes the nuclear translocation of the p65 subunit of NF-κB and induces phosphorylation of IKKβ, thereby facilitating the up-regulation of the NF-κB pathway [30]. The role of AHNAK2 in PC is rarely reported. According to the literature, bioinformatic analysis revealed that AHNAK2, TMPRSS4, POSTN, ECT2, and SERPINB5 genes have high sensitivity and specificity in the diagnosis of pancreatic cancer [31]. In addition, the analysis of the TCGA database revealed that unfavorable clinical prognosis of PC is linked with increased expression of AHNAK2 mRNA [32]. However, the connection between AHNAK2 and chemoresistance in PC, along with its underlying mechanism, remains unexplored and unreported.

This study employed transcriptome sequencing analysis to examine the gene expression patterns of gemcitabine-resistant and parental PC cell lines. The analysis revealed that 961 genes including AHNAK2, exhibited up-regulation in the gemcitabine-resistant PC cell line. By integrating the analysis of OS and PFS-related genes in TCGA-PAAD with the examination of differentially expressed genes in the GSE106336 chip, a total of 4 genes (AHNAK2, ARHGAP29, CDA, and SAMD9) were identified. In the transcriptome sequencing results, AHNAK2 expression was the highest. Therefore, the AHNAK2 gene was selected for further investigation in this study. Additional analysis of gene mutations within the TCGA-PAAD database revealed a noteworthy connection between the heightened expression of the AHNAK2 gene and the presence of KRAS and TP53 mutant genes in PC. KRAS mutation serves as a pivotal instigating and propelling factor in PC development. Moreover, the significant association between AHNAK2 overexpression and KRAS mutation underscores the critical role of AHNAK2 as a prominent oncogene in PC.

To investigate the correlation between the AHNAK2 gene and clinicopathological characteristics, as well as the prognosis of patients with PC, our study employed diverse research methods. Initially, we conducted an analysis utilizing the MEXPRESS database where we observed a strong association between the expression level of AHNAK2 and various histological types, Grade classification, N Stage, and OS in patients with PC. To further enhance the reliability of our findings, we analyzed the TCGA-PADD sample data, which consistently demonstrated that elevated AHNAK2 expression was closely linked to unfavorable OS, DFI, PFI, and DSS. To further investigate the clinical prognostic value of AHNAK2 in patients with PC, we performed immunohistochemical analysis on a total of 90 PC tissues and 80 adjacent normal tissues. Our results substantiated that AHNAK2 was prominently upregulated in PC tissues compared to adjacent normal pancreatic tissues. Notably, patients with high AHNAK2 expression showcased a shortened OS, with this correlation being associated with serum CA199 levels and N stage. Further analysis idntified significant disparities in Clinical stage, N stage, and serum CA199 levels between the PC patients with high and low AHNAK2 expression. In conclusion, AHNAK2, a proto-oncogene highly expressed in PC, is closely related to gemcitabine chemoresistance. It exhibits a remarkable specificity, and its expression correlates with the clinicopathological features and clinical prognosis of individuals diagnosed with PC.

The role of AHNAK2 remains unclear in PC and its association with gemcitabine resistance. This study aimed to analyze the enrichment of AHNAK2 single gene using GSEA pathway analysis, as well as the co-expressed genes using GO and KEGG enrichment. The expression of AHNAK2 was found to be significantly high, and the enrichment analysis revealed an involvement of AHNAK2 in various molecular functions, including cadherin binding, mediation of cell-cell adhesion, binding of cell adhesion molecules, and mediator activity in intercellular adhesion. The enrichment results of BP, CC, and MF of AHNAK2 co-expressed genes also indicated their significant involvement in cell adhesion, cell surface molecules, integrin binding, and protein tyrosine kinase signaling pathways. Cell-cell adhesion, which is a fundamental biological process in living organisms, is accompanied by signal transduction and regulation of gene expression, thereby maintaining the body's internal environment homeostasis [33]. Integrins, as crucial adhesion molecules, transmit extracellular signals into cells through various signaling pathways, leading to alterations in cell behavior (like actin reorganization, migration, and gene expression) [34]. Additionally, cadherin-related proteins activate nuclear signaling to promote cell growth, migration, and are closely related to EMT in tumors [35]. In our study, AHNAK2 expression enhanced cell-cell or cell-extracellular matrix (ECM) adhesion to promote tumor signaling pathways and cancer progression. In addition, the pentose phosphate pathway, p53 signaling pathway, basal transcription factors, galactose metabolism, and other pathway gene sets were upregulated and significantly enriched when AHNAK2 was highly expressed. Enriched pathways in Fig. 5 such as keratinocyte proliferation, embryonic skeletal system development, regulation of epidermal development, and spindle organization are related to cell proliferation and differentiation. Cell proliferation and differentiation are critical for tumor progress, as rapid and dysregulated cell growth is a hallmark of pancreatic cancer [36,37]. Additionally, the literature suggests that inhibition of NAMPT, the rate-limiting enzyme of NAD metabolic process, by the inhibitor FK866 can enhance the efficacy of gemcitabine [38]. Many studies have shown that p53 is involved in regulating drug resistance [39]. p53 signaling pathway regulates cell cycle and apoptosis, which are crucial for the drug resistance of pancreatic cancer [40,41]. According to the literature, ECM-receptor interaction and cell adhesion molecule binding induce the release of soluble factors responsible for immune evasion and ECM remodeling, which further contribute to therapy resistance [42].

The enrichment analysis of AHNAK2 co-expressed genes in Fig. 6 provides profound insights into the molecular mechanisms contributing to pancreatic cancer aggressiveness and potential drug resistance. The significant enrichment in pathways such as signal transduction, cell adhesion, and transmembrane receptor protein tyrosine kinase signaling are related to tumor metastasis and invasion [13]. Additionally, the involvement in inflammatory response pathways suggests a modulation of the tumor microenvironment [13], potentially promoting tumor growth and immune evasion. The prominence of receptor and protein tyrosine kinase activities aligns with known oncogenic signaling pathways that drive pancreatic cancer progression and contribute to resistance to therapies [14,15]. Notably, the enrichment in the PI3K-AKT signaling pathway is critical for gemcitabine resistance in pancreatic cancer [16]. These findings, consistent with known features of pancreatic cancer, suggest that targeting AHNAK2 and its associated pathways could offer new therapeutic avenues for overcoming the aggressiveness and drug resistance characteristic of this malignancy.

The overlapping pathways between Figs. 6 and 7 reveal crucial intersections in the molecular landscape of pancreatic cancer, particularly concerning AHNAK2. Both figures underscore the significance of cell adhesion and signaling pathways, indicative of the

intricate communication networks pivotal in cancer progression. AHNAK2 co-expressed genes, as depicted in Fig. 6, show enrichment in pathways associated with cell adhesion molecules, chemokine signaling, and receptor-mediated signaling, which aligns with the broader cellular interactions emphasized in key module two of Fig. 7. Moreover, the involvement of inflammatory responses and immune signaling pathways in Fig. 6 resonates with the complex interplay between the tumor microenvironment and cancer cells, an aspect that intersects with cell signaling pathways highlighted in Fig. 7. This convergence underscores the multifaceted nature of pancreatic cancer progression, where AHNAK2 serves as a central player in orchestrating diverse cellular processes critical for tumor development and dissemination.

The interaction between the immune system and cancer is intricate and involves the impact of chemotherapy drugs. Immunomodulatory cells exert an inhibitory effect on the anti-tumor response, while immune effector cells identify and eliminate tumor cells, triggering inflammation through the immune response system that inadvertently supports tumor growth. Notably, $CD4^+$ Treg cells possess potent immunosuppressive capabilities, thus fostering tumor advancement by impeding the efficacy of anti-tumor treatment [43,44]. Regulatory T (Treg) cells, known for their immunosuppressive functions, have been implicated in promoting tumor immune evasion and resistance to various cancer therapies [17]. Studies have shown that increased infiltration of Tregs within the tumor microenvironment correlates with poor prognosis and resistance to chemotherapy and immunotherapy in multiple cancer types, including pancreatic cancer [18]. Tregs suppress effector T cell functions, impede antitumor immune responses, and contribute to the establishment of an immunosuppressive niche within the tumor [18]. It has been reported in the literature that in pancreatic cancer, gemcitabine inhibits Treg infiltration in pancreatic cancer tissues and upregulates the effector T cell/Treg ratio [19]. Our study found that pancreatic cancer tissues with high AHNAK2 expression had an increased proportion of Tregs. Therefore, it is speculated that AHNAK2 and gemcitabine resistance may be related to Treg.

Our study found that AHNAK2 gene expression in PC was closely related to B cell humoral immunity, cellular immunity, macrophage polarization, and other immune processes. In contrast to the low AHNAK2 expression group, the high AHNAK2 expression group exhibited an infiltration of Treg cells, M0 macrophages, and M2 macrophages. M1 macrophages secrete reactive oxygen/nitrogen species and pro-inflammatory cytokines as weapons against tumor cells. On the other hand, M2 macrophages secrete anti-inflammatory cytokines (like IL-10, IL-1, and TGF-β) that fuel tumor growth, bolster treatment resistance, foster angiogenesis, facilitate migration and metastasis, and activate immune suppression [45]. Pancreatic cancer is characterized by massive infiltration of tumor-associated macrophages (TAMs) that drive resistance to gemcitabine [20]. Macrophages, particularly the M2 subtype, are known to promote tumor progression, metastasis, and resistance to therapy in various cancers, including pancreatic cancer [21]. These macrophages secrete cytokines and growth factors that support tumor cell survival, angiogenesis, and extracellular matrix remodeling, contributing to therapy resistance [21]. Our study demonstrates that macrophage infiltration is elevated in pancreatic cancer tissues with high AHNAK2 expression. Future research elucidating the underlying mechanisms could pave the way for novel treatment strategies for pancreatic cancer.

According to the analysis from the TIMER database, the AHNAK2 gene expression exhibits a positively correlated with the immunoregulatory suppressor gene TGFB1, while displaying a negative correlated with CD160. Furthermore, it demonstrates a positive correlation with the expression of immunomodulatory stimulator genes such as NT5E, CD276, and RAET1E. Deeper scrutiny reveals a significant positive association between the expression level of AHNAK2 gene and that of immune checkpoint inhibitory molecules like CD276, TGFB1, VEGFA, along with a negative correlation with the expression of immune checkpoint inhibitory molecule ARG1. Concurrently, the level of AHNAK2 gene expression showcases a positive relationship with the expression levels of immune checkpoint stimulating molecules such as IL1A, TNFSF9, TNFSF4, CD70, and HMGB1 while being inversely correlated with the expression level of SELP. The expression of the AHNAK2 is intricately linked to immunomodulatory genes and immune checkpoint genes in PC, potentially serving as a pivotal target for immunomodulation in this context. Consequently, AHNAK2 actively participates in and regulates immune cell infiltration in PC, intricately interwoven with immunomodulatory genes and immune checkpoint molecules. Given the substantial expression of gemcitabine-resistant AHANK2 in PC, it is conceivable that the influence of AHNAK2 extends to the antitumor efficacy of gemcitabine, potentially through the modulation of immune cell infiltration and immune regulation with the intricate landscape of the TME.

In this study, several methodological strengths were leveraged, including the integration of multiple databases such as TCGA, MEXPRESS, CIBERSORT, and TIMER, which provided robust and comprehensive data for analysis. The combination of transcriptome sequencing, tissue microarray analysis, and bioinformatics tools ensured the depth and breadth of the research. Functional validation through AHNAK2 knockdown experiments in cell lines confirmed its role in cell proliferation, colony formation, and gemcitabine sensitivity, enhancing the credibility of the findings. Furthermore, the correlation between AHNAK2 expression and clinical features, as well as immune infiltration, highlights its potential clinical relevance. However, there are some limitations. The reliance on in vitro experiments without in vivo or clinical sample validation may limit the translational potential of the findings. Additionally, the study focused primarily on gemcitabine without exploring resistance mechanisms to other chemotherapeutic agents. Despite revealing the association of AHNAK2 with the KRAS/p53 signaling pathway, the underlying molecular mechanisms remain incompletely understood.

In conclusion, AHNAK2 exhibits heightened expression in PC tissues and significantly correlates with gemcitabine resistance, different histological types, Grades, clinical Stage, N stage, and clinical prognosis of PC. Therefore, AHNAK2 emerges as a pivotal molecular marker within the realm of PC, offering the potential for clinical application in diagnosis and prognosis assessment. Furthermore, we also elucidate the intricate link between AHNAK2 and tumor immune infiltration. AHNAK2, through its regulatory impact on immune infiltration, influences the PC tumor microenvironment. This process promotes PC progression and affects the efficacy of gemcitabine. Our study introduces novel potential indicators for predicting patient survival and provides foundational research data for developing fresh immunotherapy targets. This paves the way for a novel avenue of personalized immunotherapy for

PC, ultimately benefiting a broader spectrum of patients. However, our study bears certain limitations. This study is grounded in the mining and analysis of pre-existing data. Although the AHNAK2 gene was screened by transcriptome sequencing, and its clinical significance and diagnostic value were verified by tissue microarray immunohistochemistry in PC, functional experiments were still lacking. Future inquiries should delve into the mechanism underpinning the role of AHNAK2 in the initiation and progression of PC, thereby furnishing more refined guidance and strategies for the management and prognostication of PC.

Funding

This research was funded by the National Natural Science Foundation of China (Grant No. 82273409), Guangdong Basic and Applied Basic Research Foundation (Grant No. 2023A1515010300and 2024A1515010673), and Guangzhou Municipal Science and Technology Project (Grant No. 2024B03J1246).

Data available statement

Data related to this study have been stored in a publicly available repository. The sequencing data in this study are available through the NCBI Sequence Read Archive under the accession number PRJNA1088773 (https://dataview.ncbi.nlm.nih.gov/object/PRJNA1088773?reviewer=jckdiqn90cgh6af7dqd5jb4879). TCGA data set can be obtained from the following website: http://cancergenome.nih.gov. GEO data set can be obtained from the following website: https://www.ncbi.nlm.nih.gov/geo/.

Ethics statement

The experimental material involved in the ethics of this study, tissue microarrays of human origin, was approved by the Ethics Committee's approval with the ethical number SHYJS-CP-1901008.

CRediT authorship contribution statement

Guangsheng Ou: Writing – original draft, Software, Methodology, Formal analysis, Conceptualization. **Zhenfeng Tian:** Writing – original draft, Visualization, Software, Methodology, Investigation. **Mingxin Su:** Visualization, Validation. **Miao Yu:** Validation. **Jin Gong:** Writing – review & editing, Supervision, Resources. **Yinting Chen:** Writing – review & editing, Supervision, Resources, Project administration, Data curation, Conceptualization.

Declaration of competing interest

The authors declare that they have no known competing financial interests or personal relationships that could have appeared to influence the work reported in this paper.

Appendix A. Supplementary data

Supplementary data to this article can be found online at https://doi.org/10.1016/j.heliyon.2024.e33687.

References

[1] R.L. Siegel, K.D. Miller, N.S. Wagle, A. Jemal, Cancer statistics, CA Cancer J Clin 73 (2023) 17–48, 2023.
[2] H. Sung, J. Ferlay, R.L. Siegel, M. Laversanne, I. Soerjomataram, A. Jemal, F. Bray, Global cancer statistics 2020: GLOBOCAN Estimates of Incidence and mortality worldwide for 36 cancers in 185 countries, CA Cancer J Clin 71 (2021) 209–249.
[3] H. Kim, K.N. Kang, Y.S. Shin, Y. Byun, Y. Han, W. Kwon, C.W. Kim, J.Y. Jang, Biomarker panel for the diagnosis of pancreatic ductal adenocarcinoma, Cancers 12 (2020).
[4] J. Xie, L. Xia, W. Xiang, W. He, H. Yin, F. Wang, T. Gao, W. Qi, Z. Yang, X. Yang, T. Zhou, G. Gao, Metformin selectively inhibits metastatic colorectal cancer with the KRAS mutation by intracellular accumulation through silencing MATE1, Proc Natl Acad Sci U S A 117 (2020) 13012–13022.
[5] D. Raj, M.-H. Yang, D. Rodgers, E.N. Hampton, J. Begum, A. Mustafa, D. Lorizio, I. Garces, D. Propper, J.G. Kench, H.M. Kocher, T.S. Young, A. Aicher, C. Heeschen, Switchable CAR-T cells mediate remission in metastatic pancreatic ductal adenocarcinoma, Gut 68 (2019) 1052–1064.
[6] P. Carotenuto, F. Amato, A. Lampis, C. Rae, S. Hedayat, M.C. Previdi, D. Zito, M. Raj, V. Guzzardo, F. Sclafani, A. Lanese, C. Parisi, C. Vicentini, I. Said-Huntingford, J.C. Hahne, A. Hallsworth, V. Kirkin, K. Young, R. Begum, A. Wotherspoon, K. Kouvelakis, S.X. Azevedo, V. Michalarea, R. Upstill-Goddard, S. Rao, D. Watkins, N. Starling, A. Sadanandam, D.K. Chang, A.V. Biankin, N.B. Jamieson, A. Scarpa, D. Cunningham, I. Chau, P. Workman, M. Fassan, N. Valeri, C. Braconi, Modulation of pancreatic cancer cell sensitivity to FOLFIRINOX through microRNA-mediated regulation of DNA damage, Nat. Commun. 12 (2021) 6738.
[7] M.J. Tu, P.Y. Ho, Q.Y. Zhang, C. Jian, J.X. Qiu, E.J. Kim, R.J. Bold, F.J. Gonzalez, H. Bi, A.M. Yu, Bioengineered miRNA-1291 prodrug therapy in pancreatic cancer cells and patient-derived xenograft mouse models, Cancer Lett. 442 (2019) 82–90.
[8] Z.L. Johnson, J.H. Lee, K. Lee, M. Lee, D.Y. Kwon, J. Hong, S.Y. Lee, Structural basis of nucleoside and nucleoside drug selectivity by concentrative nucleoside transporters, Elife 3 (2014) e03604.
[9] M. Liu, Y. Zhang, J. Yang, X. Cui, Z. Zhou, H. Zhan, K. Ding, X. Tian, Z. Yang, K.A. Fung, B.H. Edil, R.G. Postier, M.S. Bronze, M.E. Fernandez-Zapico, M. P. Stemmler, T. Brabletz, Y.P. Li, C.W. Houchen, M. Li, ZIP4 increases expression of transcription factor ZEB1 to promote integrin α3β1 signaling and inhibit expression of the gemcitabine transporter ENT1 in pancreatic cancer cells, Gastroenterology 158 (2020) 679–692.e671.

[10] S.W. Hung, S. Marrache, S. Cummins, Y.D. Bhutia, H. Mody, S.B. Hooks, S. Dhar, R. Govindarajan, Defective hCNT1 transport contributes to gemcitabine chemoresistance in ovarian cancer subtypes: overcoming transport defects using a nanoparticle approach, Cancer Lett. 359 (2015) 233–240.
[11] H. Han, S. Li, Y. Zhong, Y. Huang, K. Wang, Q. Jin, J. Ji, K. Yao, Emerging pro-drug and nano-drug strategies for gemcitabine-based cancer therapy, Asian J. Pharm. Sci. 17 (2022) 35–52.
[12] C.L. Costantino, A.K. Witkiewicz, Y. Kuwano, J.A. Cozzitorto, E.P. Kennedy, A. Dasgupta, J.C. Keen, C.J. Yeo, M. Gorospe, J.R. Brody, The role of HuR in gemcitabine efficacy in pancreatic cancer: HuR Up-regulates the expression of the gemcitabine metabolizing enzyme deoxycytidine kinase, Cancer Res. 69 (2009) 4567–4572.
[13] A.W. Blackstock, H. Lightfoot, L.D. Case, J.E. Tepper, S.K. Mukherji, B.S. Mitchell, S.G. Swarts, S.M. Hess, Tumor uptake and elimination of 2',2'-difluoro-2'-deoxycytidine (gemcitabine) after deoxycytidine kinase gene transfer: correlation with in vivo tumor response, Clin. Cancer Res. 7 (2001) 3263–3268.
[14] Y.T. Chang, H.Y. Peng, C.M. Hu, S.C. Huang, S.C. Tien, Y.M. Jeng, Pancreatic cancer-derived small extracellular vesical Ezrin regulates macrophage polarization and promotes metastasis, Am. J. Cancer Res. 10 (2020) 12–37.
[15] M.H. Sherman, G.L. Beatty, Tumor microenvironment in pancreatic cancer pathogenesis and therapeutic resistance, Annu. Rev. Pathol. 18 (2023) 123–148.
[16] Y. Yan, R. Gao, T.L.P. Trinh, M.B. Grant, Immunodeficiency in pancreatic adenocarcinoma with diabetes revealed by comparative genomics, Clin. Cancer Res. 23 (2017) 6363–6373.
[17] Z.M. Ye, L.J. Li, M.B. Luo, H.Y. Qing, J.H. Zheng, C. Zhang, Y.X. Lu, Y.M. Tang, A systematic review and network meta-analysis of single nucleotide polymorphisms associated with pancreatic cancer risk, Aging (Albany NY) 12 (2020) 25256–25274.
[18] S. Roth, K. Zamzow, M.M. Gaida, M. Heikenwälder, C. Tjaden, U. Hinz, P. Bose, C.W. Michalski, T. Hackert, Evolution of the immune landscape during progression of pancreatic intraductal papillary mucinous neoplasms to invasive cancer, EBioMedicine 54 (2020) 102714.
[19] B. Shi, J. Chu, T. Huang, X. Wang, Q. Li, Q. Gao, Q. Xia, S. Luo, The scavenger receptor MARCO expressed by tumor-associated macrophages are highly associated with poor pancreatic cancer prognosis, Front. Oncol. 11 (2021) 771488.
[20] A. El-Kenawi, W. Dominguez-Viqueira, M. Liu, S. Awasthi, J. Abraham-Miranda, A. Keske, K.K. Steiner, L. Noel, A.N. Serna, J. Dhillon, R.J. Gillies, X. Yu, J. M. Koomen, K. Yamoah, R.A. Gatenby, B. Ruffell, Macrophage-derived cholesterol contributes to therapeutic resistance in prostate cancer, Cancer Res. 81 (2021) 5477–5490.
[21] D. Oelschlaegel, T. Weiss Sadan, S. Salpeter, S. Krug, G. Blum, W. Schmitz, A. Schulze, P. Michl, Cathepsin inhibition modulates metabolism and polarization of tumor-associated macrophages, Cancers (2020) 12.
[22] T.A. Davis, B. Loos, A.M. Engelbrecht, AHNAK: the giant jack of all trades, Cell. Signal. 26 (2014) 2683–2693.
[23] Z. Tian, Y. Tan, X. Lin, M. Su, L. Pan, L. Lin, G. Ou, Y. Chen, Arsenic trioxide sensitizes pancreatic cancer cells to gemcitabine through downregulation of the TIMP1/PI3K/AKT/mTOR axis, Transl. Res. (2022).
[24] A.M. Newman, C.L. Liu, M.R. Green, A.J. Gentles, W. Feng, Y. Xu, C.D. Hoang, M. Diehn, A.A. Alizadeh, Robust enumeration of cell subsets from tissue expression profiles, Nat. Methods 12 (2015) 453–457.
[25] A. Komuro, Y. Masuda, K. Kobayashi, R. Babbitt, M. Gunel, R.A. Flavell, V.T. Marchesi, The AHNAKs are a class of giant propeller-like proteins that associate with calcium channel proteins of cardiomyocytes and other cells, Proc Natl Acad Sci U S A 101 (2004) 4053–4058.
[26] M. Zardab, K. Stasinos, R.P. Grose, H.M. Kocher, The obscure potential of AHNAK2, Cancers (2022) 14.
[27] M. Wang, X. Li, J. Zhang, Q. Yang, W. Chen, W. Jin, Y.R. Huang, R. Yang, W.Q. Gao, AHNAK2 is a novel prognostic marker and oncogenic protein for clear cell renal cell carcinoma, Theranostics 7 (2017) 1100–1113.
[28] M. Li, Y. Liu, Y. Meng, Y. Zhu, AHNAK nucleoprotein 2 performs a promoting role in the proliferation and migration of uveal melanoma cells, Cancer Biother. Radiopharm. 34 (2019) 626–633.
[29] G. Liu, Z. Guo, Q. Zhang, Z. Liu, D. Zhu, AHNAK2 promotes migration, invasion, and epithelial-mesenchymal transition in lung adenocarcinoma cells via the TGF-β/smad3 pathway, OncoTargets Ther. 13 (2020) 12893–12903.
[30] R. Ye, D. Liu, H. Guan, N. AiErken, Z. Fang, Y. Shi, Y. Zhang, S. Wang, AHNAK2 promotes thyroid carcinoma progression by activating the NF-κB pathway, Life Sci. 286 (2021) 120032.
[31] M.K. Bhasin, K. Ndebele, O. Bucur, E.U. Yee, H.H. Otu, J. Plati, A. Bullock, X. Gu, E. Castan, P. Zhang, R. Najarian, M.S. Muraru, R. Miksad, R. Khosravi-Far, T. A. Libermann, Meta-analysis of transcriptome data identifies a novel 5-gene pancreatic adenocarcinoma classifier, Oncotarget 7 (2016) 23263–23281.
[32] H. Klett, H. Fuellgraf, E. Levit-Zerdoun, S. Hussung, S. Kowar, S. Küsters, P. Bronsert, M. Werner, U. Wittel, R. Fritsch, H. Busch, M. Boerries, Identification and validation of a diagnostic and prognostic multi-gene biomarker panel for pancreatic ductal adenocarcinoma, Front. Genet. 9 (2018) 108.
[33] S.Y. Park, H.S. Kim, N.H. Kim, S. Ji, S.Y. Cha, J.G. Kang, I. Ota, K. Shimada, N. Konishi, H.W. Nam, S.W. Hong, W.H. Yang, J. Roth, J.I. Yook, J.W. Cho, Snail1 is stabilized by O-GlcNAc modification in hyperglycaemic condition, Embo j 29 (2010) 3787–3796.
[34] A. Leyme, A. Marivin, L. Perez-Gutierrez, L.T. Nguyen, M. Garcia-Marcos, Integrins activate trimeric G proteins via the nonreceptor protein GIV/Girdin, J. Cell Biol. 210 (2015) 1165–1184.
[35] H. Zhao, C. Diao, X. Wang, Y. Xie, Y. Liu, X. Gao, J. Han, S. Li, LncRNA BDNF-AS inhibits proliferation, migration, invasion and EMT in oesophageal cancer cells by targeting miR-214, J. Cell Mol. Med. 22 (2018) 3729–3739.
[36] Y. Ma, W. Yu, A. Shrivastava, R.K. Srivastava, S. Shankar, Inhibition of pancreatic cancer stem cell characteristics by α-Mangostin: molecular mechanisms involving Sonic hedgehog and Nanog, J. Cell Mol. Med. 23 (2019) 2719–2730.
[37] Y. Zhao, X. Li, H. Zhang, M. Yan, M. Jia, Q. Zhou, A transcriptome sequencing study on genome-wide gene expression differences of lung cancer cells modulated by fucoidan, Front. Bioeng. Biotechnol. 10 (2022) 844924.
[38] H.Q. Ju, Z.N. Zhuang, H. Li, T. Tian, Y.X. Lu, X.Q. Fan, H.J. Zhou, H.Y. Mo, H. Sheng, P.J. Chiao, R.H. Xu, Regulation of the Nampt-mediated NAD salvage pathway and its therapeutic implications in pancreatic cancer, Cancer Lett. 379 (2016) 1–11.
[39] X. Cao, J. Hou, Q. An, Y.G. Assaraf, X. Wang, Towards the overcoming of anticancer drug resistance mediated by p53 mutations, Drug Resist Updat 49 (2020) 100671.
[40] X. Wang, Y. Zheng, Y. Wang, PEAK1 promotes invasion and metastasis and confers drug resistance in breast cancer, Clin. Exp. Med. 22 (2022) 393–402.
[41] M. Yeon, S. Lee, J.E. Lee, H.S. Jung, Y. Kim, D. Jeoung, CAGE-miR-140-5p-Wnt1 Axis regulates autophagic flux, tumorigenic potential of mouse colon cancer cells and cellular interactions mediated by exosomes, Front. Oncol. 9 (2019) 1240.
[42] K. Khalaf, D. Hana, J.T. Chou, C. Singh, A. Mackiewicz, M. Kaczmarek, Aspects of the tumor microenvironment involved in immune resistance and drug resistance, Front. Immunol. 12 (2021) 656364.
[43] X. Chen, Y. Du, Q. Hu, Z. Huang, Tumor-derived CD4+CD25+regulatory T cells inhibit dendritic cells function by CTLA-4, Pathol. Res. Pract. 213 (2017) 245–249.
[44] H. Nishikawa, S. Sakaguchi, Regulatory T cells in tumor immunity, Int. J. Cancer 127 (2010) 759–767.
[45] S. Yu, H. Ge, S. Li, H.J. Qiu, Modulation of macrophage polarization by viruses: turning off/on host antiviral responses, Front. Microbiol. 13 (2022) 839585.